Structure-function studies on enzymes of the methionine salvage pathway in *Bacillus subtilis*

（枯草菌のメチオニン回収経路で機能する酵素群の構造と機能に関する研究）

Haruka Tamura

Osaka University

2009

Preface

The studies presented here have been carried out under the direction of Professor Yasushi Kai from 2006 to 2007, Professor Susumu Kuwabata from 2007 to 2008, and Professor Tsuyoshi Inoue from 2008 to 2009 at Department of Applied Chemistry, Graduate School of Engineering, Osaka University, Japan.

The object of this thesis is focused on structure-function studies of enzymes in the methionine salvage pathway from *Bacillus subtilis*. The author hopes these insights would contribute to the knowledge of novel reaction schemes and further applications for higher CO_2-fixation to establish a sustainable development on the earth.

Haruka Tamura

Department of Applied Chemistry

Graduate School of Engineering

Osaka University

Suita, Osaka

Japan

March, 2009

Table of Contents

Abbreviations

MTA	methylthioadenosine
MSP	methionine salvage pathway
M1Pi	5-methylthioribose 1-phosphate isomerase
MTR-1-P	5-methylthioribose 1-phosphate
MTRu-1-P	5-methylthioribulose 1-phosphate
IF	translation initiation factor
IF2B	including initiation factor 2B
2CABP	2-carboxy-D-arabinitol-1,5-diphosphate;
4CABP	4-carboxy-D-arabinitol-1,5-diphosphate
DK-MTP-1P	2,3-diketo-5-methylthiopentyl-1-phosphate
RuBisCO	D-ribulose-1,5-bisphosphate carboxylase/oxygenase
RLP	RuBisCO-like protein
XuBP	D-xylulose-1,5-bisphosphate.

Footnote

In Chapter I, coordinates and structure factors have been deposited in the Protein Data Bank with accession codes 2YRF for sulfate-bound M1Pi, and 2YVK for MTRu-1-P-bound M1Pi, respectively.

In Chapter II, coordinate and structure factor have been deposited in the Protein Data Bank with accession code 2ZVI for the apo, decarbamylated DK-MTP-1P enolase.

General Introduction

Methionine is an essential amino acid for a number of crucial cellular functions, including the initiation of protein synthesis, methylation of DNA and rRNA, and biosynthesis of cysteine, phospholipids, and polyamines (1). The biosynthesis of the polyamines is involved in the control of many biological processes such as carcinogenesis, cell growth and differentiation. In polyamine synthesis of spermidine and spermine, methionine is consumed in a one-to-one stoichiometry with the by-product formation of methylthioadenosine (MTA) (2). Since the amount of methionine in cells is typically limiting. Additionally, *de novo* synthesis of methionine is energetically expensive. Therefore, it is essential to salvage methionine, recycle the sulfur atom from MTA (3).

Methionine salvage pathway (MSP) is an important metabolic pathway in maintaining the amount of intravital methionine, which is frequent in Bacteria (and in Eukarya) (4, 5). MSP has attracted much attention, as one of the genes (MTA phosphorylase) in this pathway acts as a tumor suppressor gene (6). Recently, we have identified five additional genes (MtnA, MtnB, MtnD, MtnW, and MtnX) in MSP from *Bacillus subtilis* (7), which revealed that MSP in *B. subtilis* was

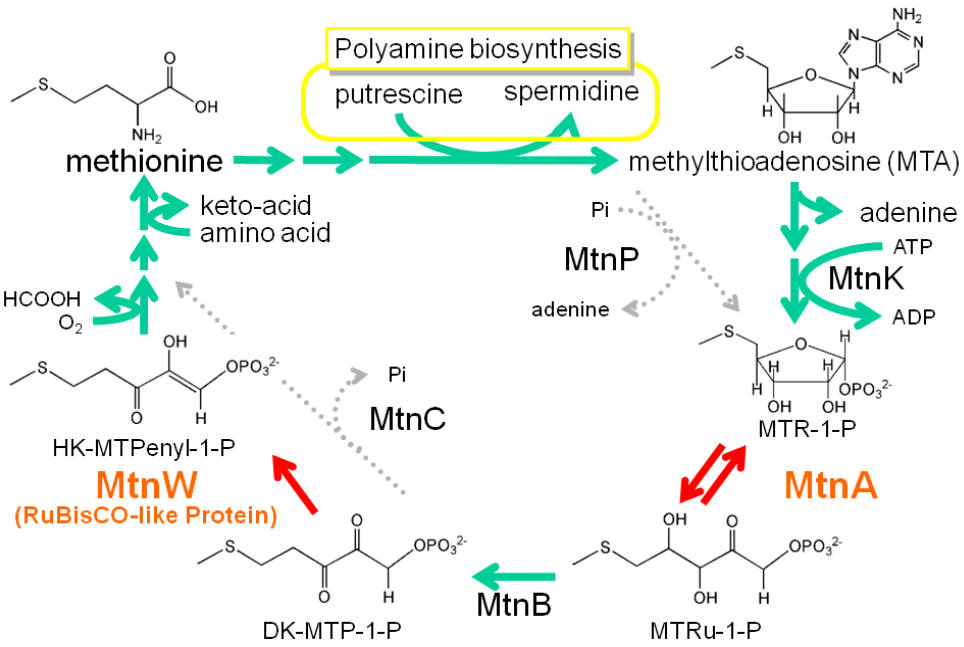

Figure 1 Methionine salvage pathway in *Bacillus subtilis* (solid line)

composed of eleven enzymes (Fig.1) (7, 8). In MSP of *B. subtilis*, MtnW has a homology to the large subunit of photosynthetic CO_2-fixation enzyme (D-ribulose-1,5-bisphosphate carboxylase/ oxygenase; RuBisCO). MtnW has been also characterized as an ancestral protein of RuBisCO because a growth-defective mutant, in which the gene for MtnW had been disrupted, was rescued by the gene for RuBisCO from the photosynthetic bacterium *Rhodospirillum rubrum* (7).

In this study, I focused on two enzymes in *B. subtilis*, MtnA (5-methylthioribose-1-phosphate isomerase; M1Pi) and MtnW (2,3-diketo-5-methylthiopentyl-1-phosphate enolase; DK-MTP-1P enolase). M1Pi and DK-MTP-1P enolase have been identified as novel enzymes, since there have been no reports about their substrates, which are used for other enzymatic reactions so far. The structural analyses of these enzymes would contribute to the knowledge of new reaction schemes and further applications for higher CO_2-fixation to establish a sustainable development.

In Chapter I, *B. subtilis* M1Pi (Bs-M1Pi; E. C. 5.3.1.23) catalyzes an interconversion of 5-methylthioribose 1-phosphate (MTR-1-P) and 5-methylthioribulose 1-phosphate (MTRu-1-P) (Fig. 1) (7). Despite structural analyses and genetic studies of homologous proteins, the catalytic mechanism of a specific isomerization by M1Pi has remained unclear. For the purpose of investigation into the detailed catalysis of M1Pi, it is crucial to analyze the crystal structures in complex with the substrate (or its analogues). In order to prepare the product complex, we had established the generation of MTR-1-P, M1Pi substrate, by using recombinant *B. subtilis* MtnK (7). Then, the crystallization of M1Pi in complex with MTR-1-P had been attempted. Herein, the crystal structures of Bs-M1Pi in complex with its product MTRu-1-P, or a sulfate have been determined at 2.4 and 2.7 Å resolution, respectively. The electron density clearly shows the presence of each compound in the active site. The structural comparison with homologous proteins enables to explain how the substrate uptake of Bs-M1Pi may be induced by an open/closed

transition of the active site. The highly conserved residue at the active site, namely Asp240 is most likely to be involved in the reaction mechanism as an acid/base catalyst. The structural analysis sheds light on its catalytic mechanism of M1Pi.

In Chapter II, *B. subtilis* DK-MTP-1P enolase (Bs-DK-MTP-1P enolase) catalyzes enolization of 2,3-diketo-5-methylthiopentyl-1-phosphate.and functions in the methionine salvage pathway (Fig.1). DK-MTP-1P enolase has attracted enormous attention because it has a homology to the large subunit of RuBisCO. RuBisCO plays a key role to fix CO_2 into a five-carbon sugar phosphate in the Calvin cycle (9). But RuBisCO is an inefficient catalyst; therefore, the development of a super-RuBisCO is a potential avenue to improve crop productivity. On the basis of structural and biochemical studies (10), DK-MTP-1P enolase catalyzes the fixation reaction of neither CO_2 nor O_2, but is considered to partially share the same activation mechanism as RuBisCO. In order to understand the functional and evolutionary relationship between RuBisCO and DK-MTP-1P enolase, the crystal structure of the apo, decarbamylated (E) form of Bs-DK-MTP-1P enolase has been determined at 2.3 Å resolution. The structural comparison with RuBisCO in the discrete catalytic steps allows to elucidate the structural consistency in DK-MTP-1P enolase and RuBisCO, providing a clue to create super RuBisCO with the ability of higher CO_2-fixation.

Chapter I

Crystal structure of 5-methylthioribose-1-phosphate isomerase from *Bacillus subtilis*: Implications for catalytic mechanism

1.1 Introduction

In MSP from *B. subtilis*, 5-methylthioribose 1-phosphate isomerase (M1Pi; E. C. 5.3.1.23) catalyzes an interconversion of 5-methylthioribose 1-phosphate (MTR-1-P) and 5-methylthioribulose 1-phosphate (MTRu-1-P) (Scheme 1-1) (7), which is classified as an aldose-ketose isomerase reaction. In general, two possible catalytic mechanisms have been proposed for an aldose-ketose isomerization (Scheme 1-2) (11). One is the *cis*-enediol mechanism that has been observed in triosephosphate isomerase, ribose 5-phosphate isomerase and phosophoglucose isomerase (11-13). These enzymes do not require any metals to exhibit their activities. The other mechanism proceeds via the hydride transfer as observed with xylose isomerase (XI) (14), which requires two divalent cations such as Mg^{2+} or Mn^{2+} (15, 16).

Scheme 1-1 5-Methylthioribose-1-phosphate isomerase (M1Pi) reaction

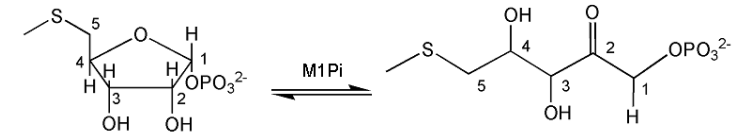

5-methylthioribose-1-phosphate (MTR-1-P) ⇌ 5-methylthioribulose-1-phosphate (MTRu-1-P)

Scheme 1-2 Mechanisms for isomerization of an aldose to a ketose.

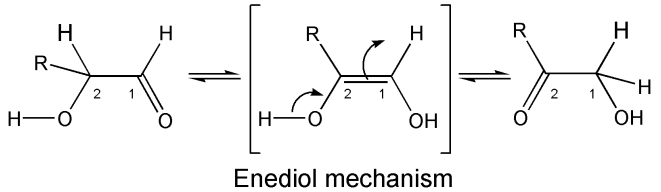

Enediol mechanism

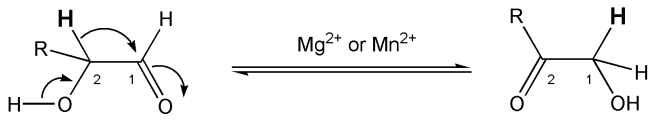

Hydride transfer mechanism

Our recent study has shown that M1Pi does not require any metals to exhibit its catalytic activity, which is analogous to the enzymes that proceed via a *cis*-enediol intermediate. However, NMR and mass spectrometry suggest the isomerase reaction of M1Pi in D_2O proceeds without incorporation of deuterium from solvent into the product (17). These spectrometric features resemble those of XI, which adopts the hydride transfer mechanism (14). Recently, Imker *et al*. has reported that Bs-M1Pi catalyzes stereospecific proton transfer via the hydride transfer mechanism by using the deuterium labeled alternative substrates, [1-^{2}H]-D-ribose-1-phopsphate and [2-^{2}H]-D-ribose-1-phosphate (10).

According to the Pfam database (18), M1Pi belongs to a large protein family related to translation initiation factor 2B alpha (PFAM family: PF01008). This family is composed of M1Pi and several translation initiation factors (IF) including initiation factor 2B (IF2B) alpha, beta and delta subunits from eukaryotes, and initiation factors 2B1 and 2B2 from Achaea (19, 20). Generally speaking, IF2B interacts with the IF2-GDP complex, which promotes guanine nucleotide exchange, while M1Pi catalyzes a specific isomerization.

Recently, high resolution crystal structures have become available for several M1Pi homologous proteins in the Protein Data Bank (PDB) (21). Although yeast Ypr118w (PDB code: 1W2W: 38% identity) has been characterized as M1Pi (22), M1Pi-related proteins of *Thermotoga maritima* (PDB code: 1T9K: 50% identity), *Pyrococcus horikoshii* OT3 (PDB code: 1VB5: 32% identity) (23) and *Archaeoglobus fulgidus* (PDB code: 1T5O: 43% identity) have been annotated as putative proteins of unknown function. At present, M1Pis from *B. subtilis* and yeast are the only enzymes, whose activities have been directly measured (7, 22). Herein, we describe the crystal structures of M1Pi from *B. subtilis* (Bs-M1Pi) in complex with its product and a sulfate, respectively. The structural analysis explains how the substrate binding may be associated with an open/closed transition of the active site and also sheds light on its reaction mechanism involving

Asp240 as a catalytic acid/base.

1.2 Materials and Methods

1.2.1 Cloning and Expression of Bs-M1Pi

The full-length M1Pi (*mtnA*) gene was amplified from genomic DNA by PCR, which was performed with the following forward and reverse primers: 5'-GGAATTCCATATGACCCAT TCATTTG CTG-3'and 5'-CGGGATCCAAATGA- GCAAAGTCC-3'. The products of PCR were digested with *Nde*I and *Bam*HI. The fragments were ligated at *Nde*I/*Bam*HI site of pET15b (Novagen).

E. coli strain BL21 (DE3) cells harboring the M1Pi expression plasmid were grown for 8 h in LB medium containing 50μg ml^{-1} ampicillin at 310 K. The cells were grown for a further 16 h at 303 K. The cells were then harvested by centrifugation at 6000*g* for 30 min. The cell pellet was resuspended in buffer *A* (50 mM Na HEPES pH 7.4, 500 mM NaCl and 10mM Imidazol) and 1 mM PMSF, then disrupted by a French Press.

1.2.2 Purification

The disrupted cells were centrifuged at 400 000g at 277 K for 30 min. The supernatant was loaded onto a 5ml HiTrap Chelating column (Amersham Pharmacia Biotech) equilibrated with buffer A. The unbound proteins were flushed with buffer A. M1Pi with a N-terminal histidine tag was eluted with a 150-225 mM imidazole gradient. Further purification to M1Pi was carried out using a HiLoad 26/60 Superdex 75 prep grade column (Amersham Pharmacia Biotech) equilibrated with 50 mM Na HEPES pH 7.4 containing 1 mM EDTA. Pooled fractions were concentrated to 30 mg ml^{-1} with Vivaspin 20 ml (5,000 MWCO PES, Vivascience), and used for crystallization without removal of the N-terminal histidine tag.

1.2.3 Crystallization

The crystallization screen of 30 mg ml^{-1} M1Pi (in 50 mM Na HEPES pH 7.4 and 1 mM EDTA) was initially performed with Crystal Screen and Crystal Screen 2 (Hampton Research) in 96-well sitting-drop plates (Corning) at 293 K. The drop size was 2 μl, with protein, reservoir ratio of 1:1. Oval shaped crystals with maximum size of 0.15 × 0.05 × 0.02 mm were obtained using Crystal Screen 2 condition No.23 [100 mM MES (pH 6.5), 1.6 M ammonium sulfate, 10% (v/v) 1,4-dioxane] within 2 weeks (Fig. 1-1A). However, the crystal diffracted with high mosaicity (1.6). Other small crystals appeared with Crystal Screen 2 condition No.42 [100 mM Tris (pH 8.5), 1.5 M ammonium sulfate, 12% (v/v) glycerol] after a month. To refine the conditions, we varied the pH, buffer, concentrations of protein or precipitant, and attempted the hanging-drop vapor-diffusion method using a 2 μl drop containing equal volumes of protein and reservoir solution suspended over 400 μl reservoir solution. Optimized crystallization was performed with the sitting-drop vapor-diffusion method at 293 K with the following: a drop (2 μl) containing equal volumes of protein (10 mg ml^{-1} M1Pi) and reservoir solution [50 mM MES, 50 mM Tris (the final pH 7.4), 1.55 M ammonium sulfate, 5% (v/v) 1,4-dioxane, 6% (v/v) glycerol] suspended over 100 μl reservoir solution. Crystals suitable for diffraction with maximum size of 0.1 × 0.05 ×0.03 mm appeared after 1 week (Fig. 1-1B).

As for preparing crystals in complex with its substrate (or product), two difficulties had to be overcome. Firstly, the substrate MTR-1-P had to be synthesized as MTR-1-P is not commercially available. Secondly, the crystallization conditions included neither phosphate nor sulfate as these compounds are generally thought to inhibit the binding of the substrate. In order to solve the first problem, we synthesized MTR-1-P from S-adenosylmethionine by using an enzyme MtnK from *B. subtilis*, as reported previously (7). MTR-1-P was then rendered salt-free by purification (24). To overcome the second obstacle, crystallization was performed in the absence of

sulfate and phosphate, although we had already obtained crystals in the presence of high concentration of sulfate. The crystals of M1Pi complexed with its products were obtained by co-crystallization with the substrate 5-methylthioribose 1-phosphate (MTR-1-P). Detailed crystallization conditions of the product complex are as follows: drops contained a 1.6:1.4 ratio (μl) of a protein solution (10 mg/ml M1Pi in 50 mM Na HEPES, pH 7.4 and 1 mM EDTA, supplemented with 33 μM MTR-1-P) and a reservoir (0.2 M K formate and 15% (w/v) polyethylene glycol 3350). Crystals suitable for diffraction with maximum size of 0.25 × 0.05 ×0.05 mm appeared after 2 weeks (Fig. 1-1C).

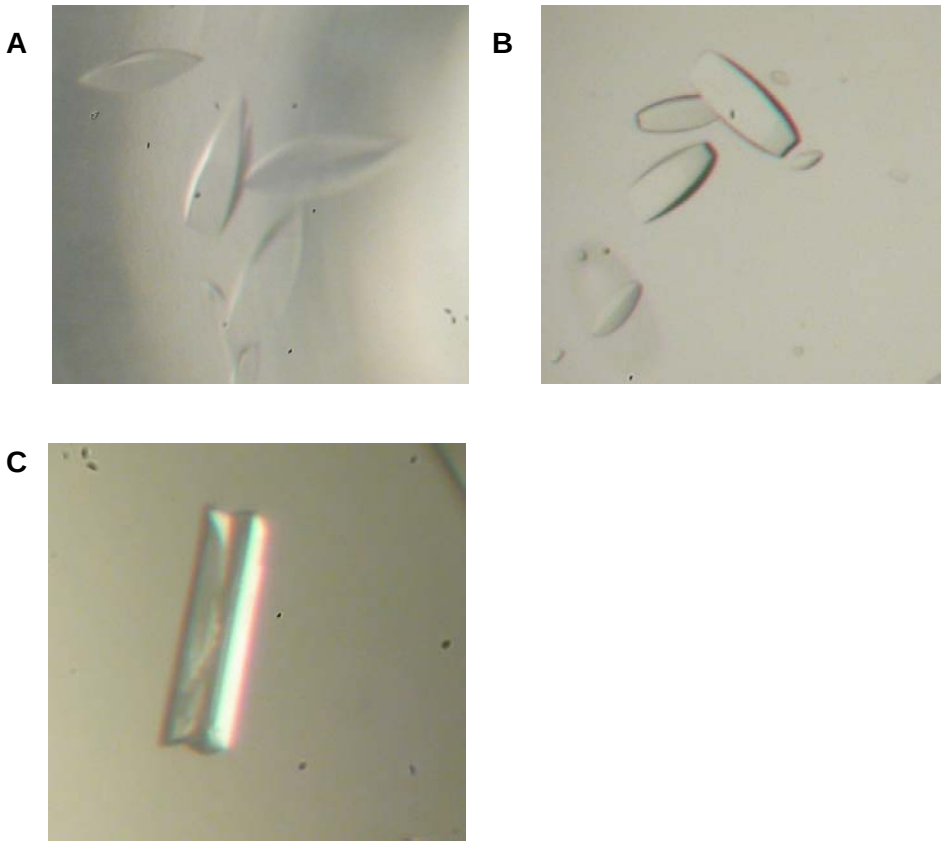

Figure 1-1 Crystals of M1Pi from *B. subtilis*.
(A) Crystals of Bs-M1Pi in the initial screening (maximum dimensions 0.15 × 0.05 × 0.02 mm). Crystals of Bs-M1Pi in complex with a sulfate ion (B), and MTRu-1-P (C). Maximum dimensions are 0.10 × 0.05 × 0.03 mm, and 0.25 × 0.05 ×0.05 mm, respectively.

1.2.4 X-ray data collection

The crystals were flash-cooled in cryo-protectant containing 20% (v/v) glycerol and 2.0 M ammonium sulfate (for sulfate complex), 20% (v/v) glycerol (for product complex), respectively. For crystals in complex with a sulfate ion, the diffraction data were collected to 2.5 Å on a Rigaku RAXIS5 detector using synchrotron radiation of wavelength 1.0 Å at the BL38B1 beamline in SPring-8 (Fig. 1-2). Data collection was performed with a total oscillation range of 180°, with a step size of 1.0° for exposure time of 100s. Crystals belonged to the space group $P4_1$ with unit-cell parameters of $a = b = 69.2$, and $c = 154.7$ Å. All diffraction data were processed using the *HKL*2000 program package (25) and the *CCP*4 program suite (26).

For crystals in complex with its product, the diffraction data were collected at the BL44XU beamline in SPring-8. Crystals belonged to the space group $P2_1$ with the cell parameters $a = 79.9$, $b = 84.4$, $c = 95.3$, $\beta = 92.4$. Diffraction data were processed with DENZO and SCALEPACK from the HKL program suite (27). The crystallographic and X-ray data statistics are summarized in Table 1-1.

1.2.5 Structure determination and Refinement

The structure of sulfate-bound M1Pi was determined by the molecular replacement method using the program MOLREP (28) with a crystal structure of Ypr118w (RCSB PDB ID: 1W2W) as a search model. The structure of MTRu-1-P-bound M1Pi was determined by molecular replacement with the sulfate-bound structure. Refinement procedures for sulfate- and MTRu-1-P-bound structures were carried out using the program CNS (29) without non-crystallographic symmetry (NCS) restrains/constraints. The structures were visualized and modified using the programs O (Alwyn Jones, Uppsala University, Sweden), and COOT (30). The final atomic coordinates and structure factor amplitudes have been identified (PDB code: 2YRF for sulfate-bound M1Pi, and

2YVK for MTRu-1-P-bound M1Pi, respectively). The final R_{work} and R_{free} are 22.5 and 28.4% for sulfate-bound M1Pi at 2.7 Å resolution, and 21.0 and 25.5% for MTRu-1-P-bound M1Pi at 2.4 Å resolution, respectively. The electron density map was clear for almost the entire polypeptide of sulfate-bound M1Pi except for first nine and last five residues, while that of MTRu-1-P complex M1Pi was clear except for last five residues, which were disordered. Pro196 is in the *cis*-conformation in both structures. The stereochemical qualities of the final structures were assessed with programs PROCHECK (31) and WHATCHECK (32). Figures were generated by MOLSCRIPT (33), RASTER3D (34) and PyMOL (35), and all structural comparisons were carried out using the program LSQKAB (26).

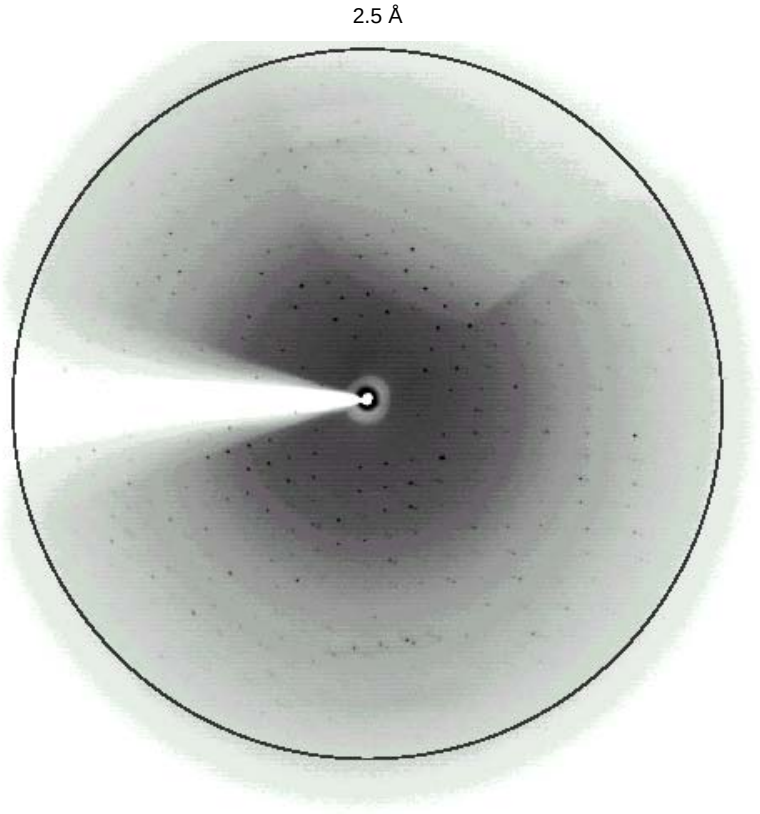

Figure 1-2 X-ray diffraction image from a sulfate ion complex M1Pi crystal

Table 1-1 Date collection and refinement statistics

	Sulfate ion complex	MTRu-1-P complex
Space group	$P4_1$	$P2_1$
Unit-cell parameters (Å, °)	$a = b = 69.2$, $c = 154.7$	a =80.0, b = 84.4, c = 95.3, β = 92.3
Resolution range (Å)	41.4- 2.70	94.9 - 2.40
No. of molecules per a. u.[a]	2	4
V_M (Å ^{3}/dalton)	2.8	2.1
V_{solv}(%)	56	41
No. of measured reflections	276,966	145,183
No. of unique reflections	18,648	49,797
$I/\sigma(I)$	24.5(3.2)[b]	30.1(3.1)[c]
R_{merge} (%)[d]	6.8(25.6) [b]	5.5(29.0) [c]
Completeness (%)	94.1(76.0) [b]	98.4(92.7) [c]
R_{cryst} (%)	22.5	21.0
R_{free} (%)	28.4	25.5
Rms deviations		
Bonds (Å)	0.011	0.007
Angles (°)	2.035	1.391

[a] asymmetric unit
[b] Values in parentheses are for the highest resolution shell (2.80 -2.70 Å)
[c] Values in parentheses are for the highest resolution shell (2.49 -2.40 Å)
[d] $R_{merge} = \Sigma|I(k)-I|/\Sigma I(k)$, where $I(k)$ is value of the kth measurement of the intensity of a reflection, I is the mean value of the intensity of that reflection and the summation is the over all measurements.

1.3 Results

1.3.1 Overall structure

The crystal structure of Bs-M1Pi co-crystallized with the substrate MTR-1-P appears to be a product MTRu-1-P complex as explained below. Firstly, a *Fo-Fc* omit map apparently revealed that the MTRu-1-P was bound to the active site (Fig. 1-3C). Secondly, the equilibrium constant, the concentration ratio [MTRu-1-P]/[MTR-1-P] at the equilibrium was 6.0 (17). The crystallization took two weeks under low salt conditions, which is long enough to reach equilibrium. The bound

species was therefore considered to be the product MTRu-1-P, not the substrate. On the other hand, the structure of sulfate-bound Bs-M1Pi shows tight binding of a sulfate at the active site, judged by the electron density (Fig. 1-3D).

The asymmetric unit (a.u.) contains two dimers for the MTRu-1-P-bound form, while one dimer is found in the a.u. for the sulfate-bound form. Each complex dimer in the a.u. is related by non-crystallographic 2-fold symmetry. In the MTRu-1-P-complex, four subunits were structurally similar, and their superposition gives a root mean square deviation (rmsd) ranging from 0.42 Å to 0.47 Å. Whereas rmsd of the two polypeptides of the sulfate-bound dimer are relatively large (with rmsd of 0.96 Å for 339 Cα atoms), because of a conformational difference in the solvent-exposed loop comprising residues 70-75 (referred to as Loop 70-75 hereafter; see Fig 1-3A). Since this region contacts with a neighboring molecule in the crystal, the structural difference is probably due to the molecular packing in the crystal. By comparing MTRu-1-P- and sulfate-bound structures, remarkable structural changes were not observed (rmsd of 0.62 Å for 333 Cα atoms) except for this loop. Therefore, we will mainly describe the crystal structure of M1Pi complexed with MTRu-1-P (Fig. 1-3A).

Similar to *yeast* M1Pi (Yw-M1Pi), each subunit can be divided into two domains, the N-terminal domain (residues 1-146) and the C-terminal domain (residues 147-353), respectively. The N-terminal domain folds into a three-stranded antiparallel β-sheet (β1-3) followed by 5 α-helices (α1-5). The intermolecular contacts within the dimer involve a part of the C-terminal region comprising residues 187-315 (α7-9 and β5-10). Tthe buried solvent-accessible surface is ~2300 $Å^2$ by calculation with GRASP (36). The C-terminal domain exhibits Rossmann-fold (αβα-sandwich; Fig. 1-3B), which participates in the binding of MTRu-1-P.

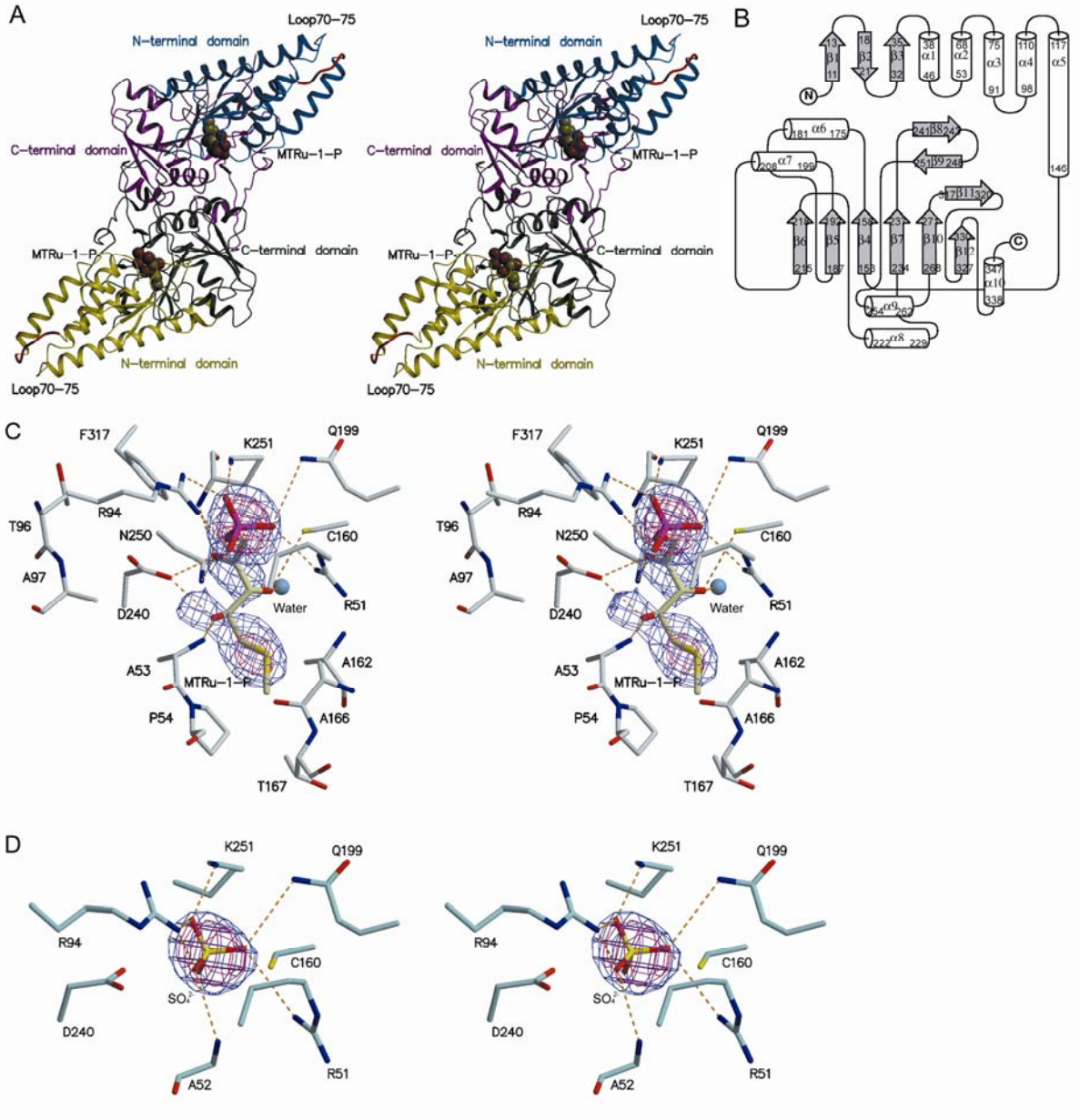

Figure 1-3 Structure of *Bacillus subtilis* M1Pi.
(A) Stereo view of the MTRu-1-P bound Bs-M1Pi dimer, viewed with the internal 2-fold axis in the perpendicular to the paper. Ribbon representation of the dimer where one subunit is colored yellow and green and the other subunit is cyan and pink. For the respective subunits, the yellow and cyan regions correspond to the N-terminal domains (residues 1-146), green and pink to the C-terminal domains (residues 147-353), respectively. Loop 70-75 is colored in red, which is observed as a most changeable region between MTRu-1-P- and sulfate-bound M1Pi structures. (B) Schematic representation of the secondary structure of Bs-M1Pi. β-strands (shaded in gray) are represented as arrows and α-helices as cylinders. Residue numbers are indicated at the start and end of each secondary structural element. The secondary structure elements were defined using the program DSSP . Stereo view showing MTRu-1-P (C) and sulfate (D) binding sites of Bs-M1Pi. The *Fo-Fc* omit maps of the compounds are countered at 1.5σ (blue) and 5σ (magenta) levels, respectively. The side chains of those residues surrounding the ligands are shown as sticks, with white and skyblue carbons (MTRu-1-P- and sulfate-bound forms, respectively), red oxygens, blue nitrogens, and yellow sulfurs. Water molecules are shown as cyan spheres. Potential hydrogen bonds are shown as orange dashed lines.

1.3.2 Active site structure

The residues involved in MTRu-1-P binding can be divided into three groups: those involved in forming hydrogen bonds with 1) the phosphate group of MTRu-1-P, and 2) the backbone oxygens or hydrogens of ribulose, and hydrophobic interactions with 3) the methylthio group (Fig. 1-4A). Superimposed structures of M1Pi complexed with MTRu-1-P and sulfate show that the phosphate group of MTRu-1-P is well-fitted onto the sulfate binding position. The side chains of Arg51, Arg94, Gln199 and Lys251 and backbone amide group of Gly52 form hydrogen bonds with the phosphate group (Fig. 1-4A). The residues involved in hydrogen bonds to carbonyl and hydroxyl oxygens of ribulose are listed as follows: the side chains of Asn250 and Asp240 form hydrogen bonds to the C2 carbonyl oxygen; the side chain of Cys160 and a water molecule interact with the C3 hydroxyl group; the side chain of Asp240, the backbone carbonyl group of Ala239, and the backbone amide group of Ala53 are hydrogen-bonded to the C4 hydroxyl group. These residues are absolutely conserved in the M1Pi family (Fig. 1-5). Of these residues, the side chain of Asp240 only interacts with both C2 carbonyl and C4 hydroxyl oxygens (Fig. 1-4A).

The hydrophobic interaction of the methylthio group includes the side chains of Pro54, Ala162, Ala166, and Thr167 (Fig. 1-4A). These residues are almost conserved in all M1Pis structures except for Ala162, which is changed to threonine in Yw-M1Pi (Fig. 1-5). Since the hydrophobic interaction occurs in Cα and Cβ carbons of Ala162 of Bs-M1Pi, Thr183 of Yw-M1Pi will probably share similar interactions to those of Ala162 in Bs-M1Pi.

The thiol group of Cys160 interacts with the C1 (3.6 Å) and C2 (3.5 Å) of MTRu-1-P through van der Waals interaction, and also makes hydrogen bonds to the amide NH group of Asn161 and ε-amino group of Arg51 (Fig. 1-4B). According to a previous computational study (37), the hydrogen bonds between the thiol group of cysteine and the amide NH group of the main chain lower the p*K*a of the thiol group by more than 1.0 pH unit. The p*K*a value of Cys160 would be

estimated at around 7, so that the thiol group of Cys160 may be deprotonated at the optimal pH of M1Pi (pH 8.1) (17). Accordingly, Cys160 is likely to stabilize δ+ formed transiently during catalysis. The side chain of Asp240 is surrounded by the hydrophobic pocket formed by residues Thr96, Ala97, and Phe317 (Fig. 1-4B and Table 1-2), which are absolutely conserved in all M1Pis (Fig. 1-5). This hydrophobic pocket appears to restrict the rotation of the Asp240 side chain, which may permit a favorable interaction with the substrate (or product). In addition, a hydrophobic environment generally allows p*K*a of the carboxyl group of aspartate to increase (38-40). For instance, the p*K*a of Asp26 buried in the hydrophobic cavity in *Escherichia coli* thioredoxin was changed from 4.4 to 7.5 (40). The p*K*a of Asp240 is likely to be increased, which might enable Asp240 to play a dual role as a proton donor/acceptor.

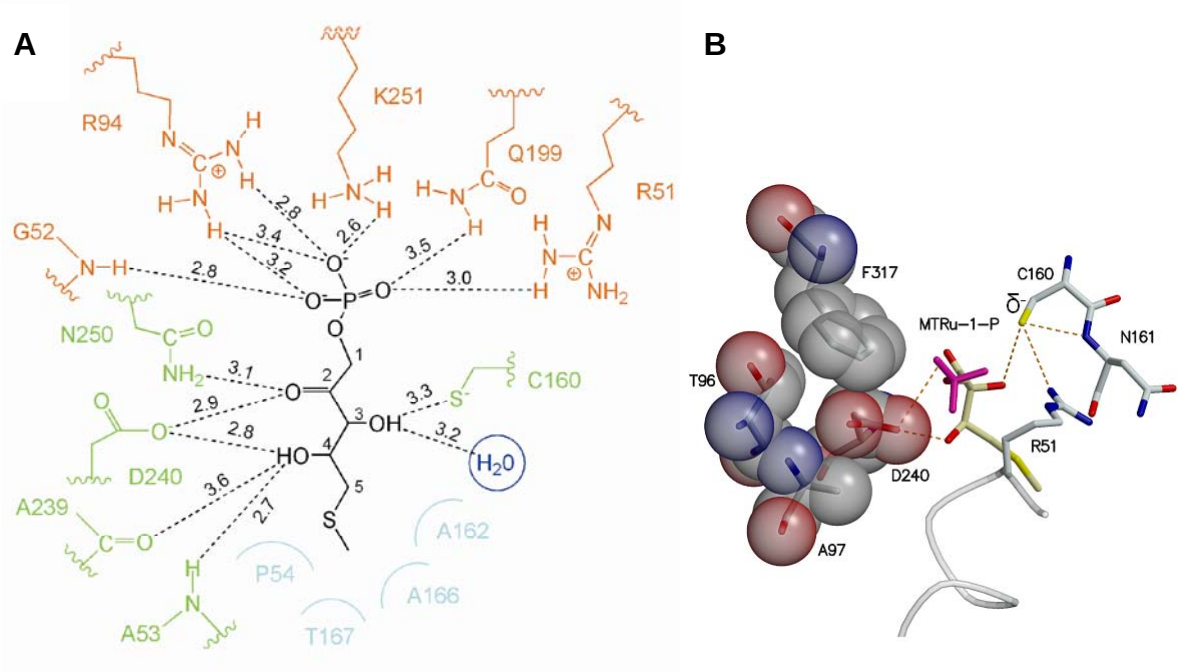

Figure 1-4 Active site structure of Bs-M1Pi
(A) Schematic drawing of the active site structure, showing the atoms and interactions around MTRu-1-P. Hydrogen bonds are indicated as dashed lines with the distance in angstroms. The hydrophobic interactions are shown as cyan semicircles. The residues involved in the binding of the phosphate group and the backbone oxygens of MTRu-1-P are shown in orange and green, respectively. (B) CPK representation of nonpolar residues (Thr96, Ala97, and Phe317) around conserved Asp240 in M1Pi. Arg51, Cys160, Asn161, and MTRu-1-P are shown as a stick model.

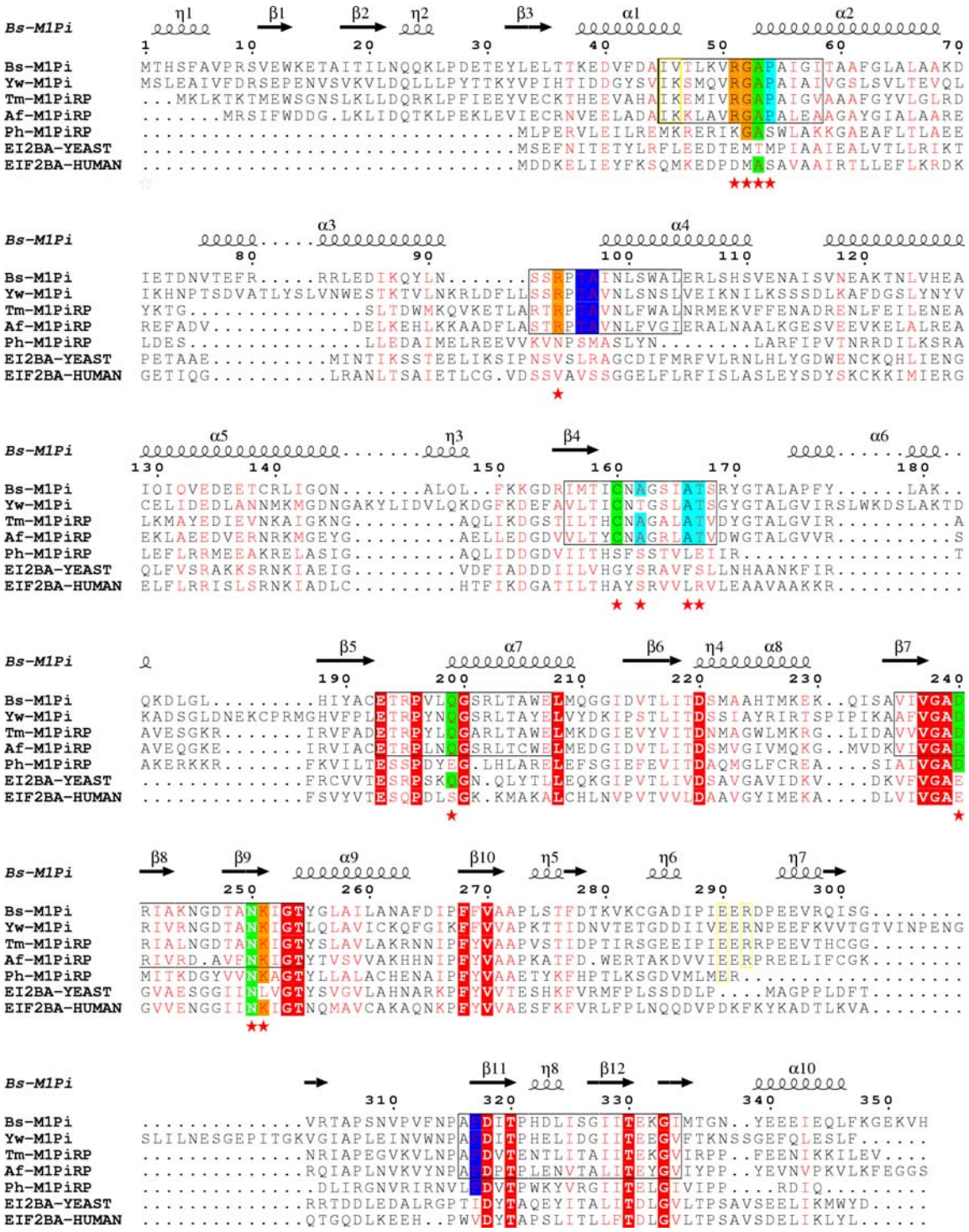

Figure 1-5 Sequence alignment of M1Pi-related proteins.
The sequences are M1Pi from *B. subtilis* (Bs-M1Pi), yeast Ypr118w (Yw-M1Pi), M1Pi-related proteins of *T. maritima* (Tm-M1PiRP), A. *fulgidus* (af-M1PiRP), *P. horikoshii* OT3 (Ph-M1PiRP), and yeast eIF-2Bα (GCN3, GenBank accession no. **NP_012951**) and human eIF-2Bα (GenBank accession no. **NP_001405**) and. Numbers above the sequences as well as the secondary structure assignment refer to the Bs-M1Pi sequence. Black boxes on the sequence indicate the position of six conserved sequence motifs. The product MTRu-1-P ligands are marked by a red star below the sequence. Residues involved in the binding of the phosphate group and the backbones of MTRu-1-P are highlighted in orange and green, respectively. The residues involved in the hydrophobic interaction are depicted in cyan. The color code is the same as Figure 1-4A. The residues with different hydrogen bonding network between open (PDB code: 1T5O) and closed (MTRu-1-P-bound Bs-M1Pi) forms are surrounded by yellow boxes.

Table 1-2 Hydrophobic interactions around Asp240

Peptide atom		Contact atom		Distance (Å)
Asp240	$O^{\delta1}$	Thr96	C^{β}	4.1
			C^{γ}	4.1
			C	3.9
		Ala97	N	3.5
			C^{α}	3.6
			C^{β}	3.1
		Phe317	$C^{\delta1}$	4.1
			$C^{\varepsilon1}$	3.5
			C^{ζ}	3.6

1.3.3 Structural comparison with other M1Pi-related proteins

To date, several crystal structures of M1Pi-related proteins have been identified in PDB. However, most of these proteins were annotated as putative translation initiation factor 2Bs (IF2Bs) or putative M1Pis despite the fact that there is no biochemical evidence. Although Yw-M1Pi (PDB code: 1W2W) has been characterized as M1Pi, M1Pi-related proteins of *T. maritima* (Tm-M1PiRP), *P. horikoshii* OT3 (Ph-M1PiRP), *A. fulgidus* (Af-M1PiRP) have been annotated as proteins of unknown function. A careful comparative analysis would help to predict their functions.

Firstly, we compared Bs-M1Pi with Yw-M1Pi as a control model. The structurally superimposed regions are composed of 153 amino acid residues, where the rmsd of the superimposed Cα atoms was calculated to be 1.0 Å. Additionally, the 13 residues in the active site of Yw-M1Pi are well superimposed on those of MTRu-1-P-bound Bs-M1Pi (rmsd of 0.5 Å for 33 atoms of side chains; Fig. 1-6A). The residues involved in ligand-binding are structurally equivalent in both complex structures, although the bound species in the active sites are different (a product for M1Pi and a sulfate for Yw-M1Pi). This analysis confirms that M1Pi shares a structurally conserved active site despite sequence divergence (Yw-M1Pi shows 38% amino acid sequence identity with Bs-M1Pi).

Secondly, we compared Bs-M1Pi with the Tm-M1PiRP, whose structure has been determined by the Midwest Center for Structural Genomics group (MCSG) and identified as a probable M1Pi in PDB. Structural comparison shows that rmsd of the superimposed Cα atoms was markedly low (1.5 Å for 322 Cα atoms). The residues involved in MTR-1-P binding are absolutely conserved and superimposed well onto those of Bs-M1Pi (rmsd of 0.7 Å for 33 side chains; Fig. 1-6A), suggesting that this protein is probably M1Pi.

On the other hand, Ph-M1PiRP seems to differ from these proteins. Although the structure can be superimposed onto Bs-M1Pi (rmsd of 1.7 Å for 222 Cα atoms) and the sequence identity is high (32%), the protein lacks residues involved in MTRu-1-P binding (Fig. 1-5). In addition, the corresponding residues in the active site are structurally rather different compared to M1Pi (Fig. 1-6B). These observations suggest that Ph-M1PiRP is not M1Pi, but probably a translational initiation factor. Finally, we have noticed that the crystal structure of Af-M1PiRP had a remarkable structural difference (rmsd of 2.2 Å for 310 Cα atoms) despite the absolute conservation of residues forming the active site (see Fig. 1-5). This Af-M1PiRP had been annotated by the New York Structural Genomics Research Consortium (NYSGRC), as a putative protein of unknown function.

It should be noted that the N-terminal and C-terminal domains of Bs-M1Pi and Af-M1PiRP can fit well separately (rmsd of 1.3 Å for 107 Cα atoms of N-terminal and 1.2 Å for 216 Cα atoms of C-terminal domains, respectively). The active site residues of each domain are also well-superimposed (rmsd values are 0.7 Å for all atoms of the active-site residues of N-terminal domain and 0.4 Å for those of C-terminal domain, respectively; Figs. 1-6C and 1-6D). These structural congruencies suggest mechanistic hypothesis, as described below.

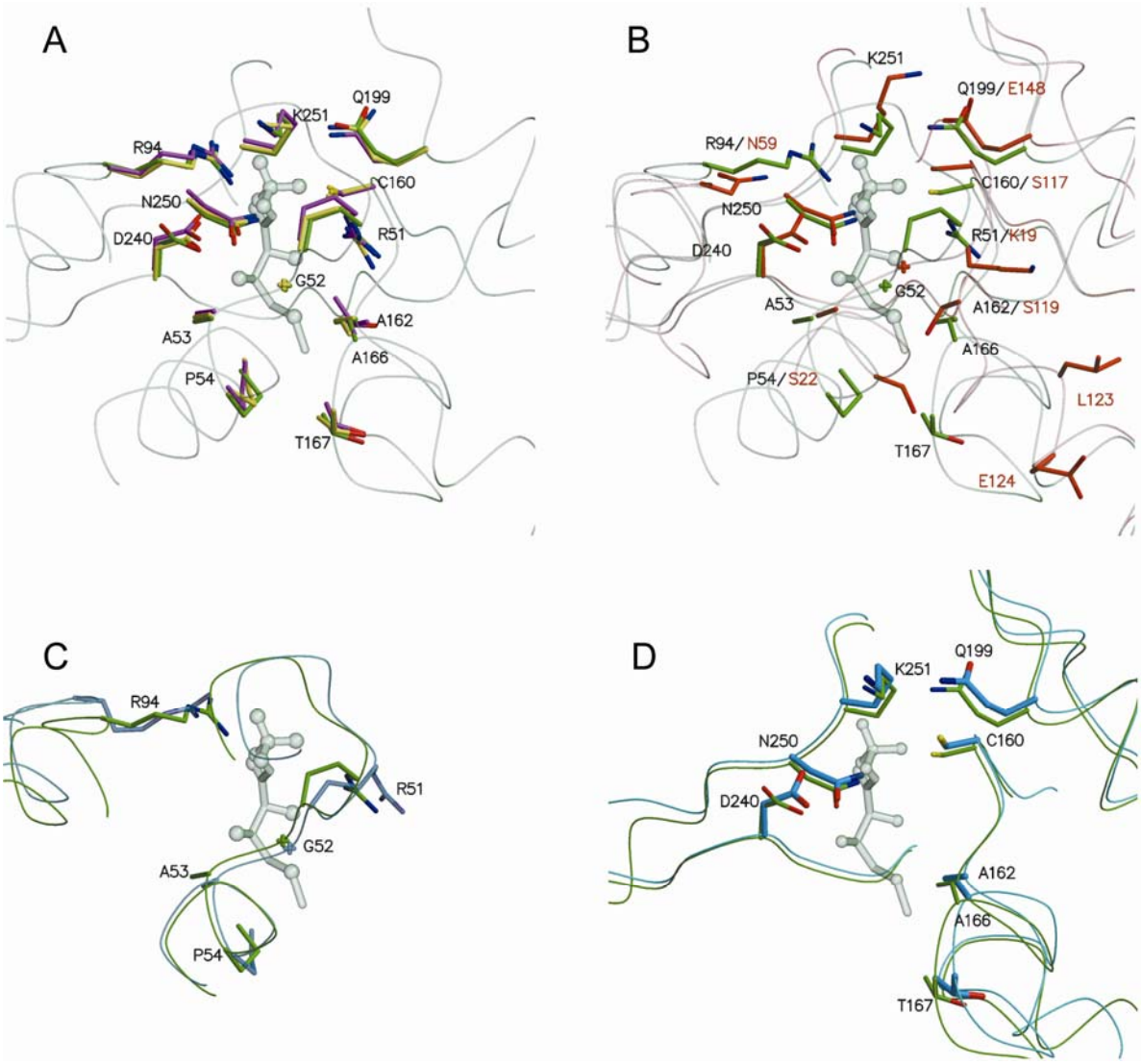

Figure 1-6 Structural comparison around the active site of M1Pi with M1Pi-related proteins.
(A) Comparison of the active sites of the Bs-M1Pi (green), yeast Ypr118w (magenta) and Tm-M1PiRP (yellow). The residues are shown as sticks, together with ribbon representation (grey). MTRu-1-P is shown in ball-and-stick representation (green transparent). Residue numbers are shown in Bs-M1Pi numbering. (B) Superposition of the active site residues in Bs-M1Pi (green) onto those of Ph-M1PiRP (orange). The amino acid residues are shown in Bs-M1Pi numbering / Ph-M1PiRP numbering. (C) Superposition of the active site residues in the N-terminal domain. The residues of Bs-M1Pi and Af-M1PiRP are shown in green and cyan, respectively. (D) Superposition of the active site residues in the C-terminal domain. The color code is the same as (C).

1.3.4 Open/closed conformational transition of M1Pi

The structure of Bs-M1Pi shows that the active site is completely shielded from the solvent region (Fig. 1-7A). On the other hand, Af-M1PiRP shows that the active site residues are highly exposed to solvent, which is probably ready to bind the substrate (or product) (Fig. 1-7B). When the conformations of MTRu-1-P bound Bs-M1Pi and unliganded Af-M1PiRP are compared by program DynDom (41), the following results were obtained. (i) The conformational changes can be described as the rigid body movement of two domains (rotation of 21°) (Fig. 1-7C). (ii) The identified two rigid domains are composed of residues 1-137 and residues 138-343, which roughly correspond to N- and C-terminal domains, respectively. (iii) The 'bending residues' between the two domains are 11 to 53, 55-56, 60-134, and 137-137, which include two phosphate binding residues (Arg51 and Lys94) in the active site. It would suggest the flexibility of active site composed of N-terminal domain. It is thus tempting to speculate that the open/closed domain motion might occur upon substrate binding, since the crystal structures of Af-M1PiRP and Bs-M1Pi shows apo and holo (MTRu-1-P-bound) forms, respectively. Structural comparison shows that the water molecules in the active site are excluded upon substrate binding and the remarkable conformational change is observed in loop 93-98 (Fig. 1-7D). The entropically favorable binding could be coupled to the exclusion of hydrophobic hydration. For instance, the colicin E9 endonuclease (E9 DNase)-immunity (Im) protein binding takes the form of rigid-body rotations and is driven through the loss of hydration (42). The changes in heat accompanying the complex binding was measured by using ITC, which shows the Im binding to the E9 DNase is entropically favored. Thus, MTRu-1-P-bound form of Bs-M1Pi appears to be tightly packed active-site, suggesting that the exclusion of water molecules from the active-site seems to stabilize entropically the active-site in the closed conformation.

As for the conformational change, loop 93-98 corresponds to one of the highest conserved

motifs among the M1Pis family (Fig. 1-5). The side chain of Arg94 on this loop participates directly in binding of the phosphate group of MTRu-1-P. This ion pair seems to lead the rearrangement of the loop 93-98 and the backbone shifts of approximately 8 Å (bottom arrow in Fig. 1-7D). Upon this conformational change, the side chain of Glu290, which originally interacted with Arg292, is also conformationally changed (top left arrow in Fig. 1-7D) to interact with the side chain of Arg94. At the same time, the conformational change of the side chain of Arg292 was also induced to interact with the backbone carbonyl of Val46 (top right arrow in Fig. 1-7D). Val46 is located at the C-terminus of α-1 helix; therefore, the side chain of Arg292 is positioned at the negative pole of theα-1 helix, which seems to stabilize the closed conformation. The residues involved in the rearrangements as described above are absolutely conserved in all M1Pis, except for Val46 (Fig. 1-5). Therefore, the substrate binding is likely to induce the large conformational changes of N- and C-terminal domains and the exclusion of water molecules from the active-site as well as the rearrangement of the hydrogen bond network around the loops 93-98 and 290-294 to stabilize the closed state of the enzyme.

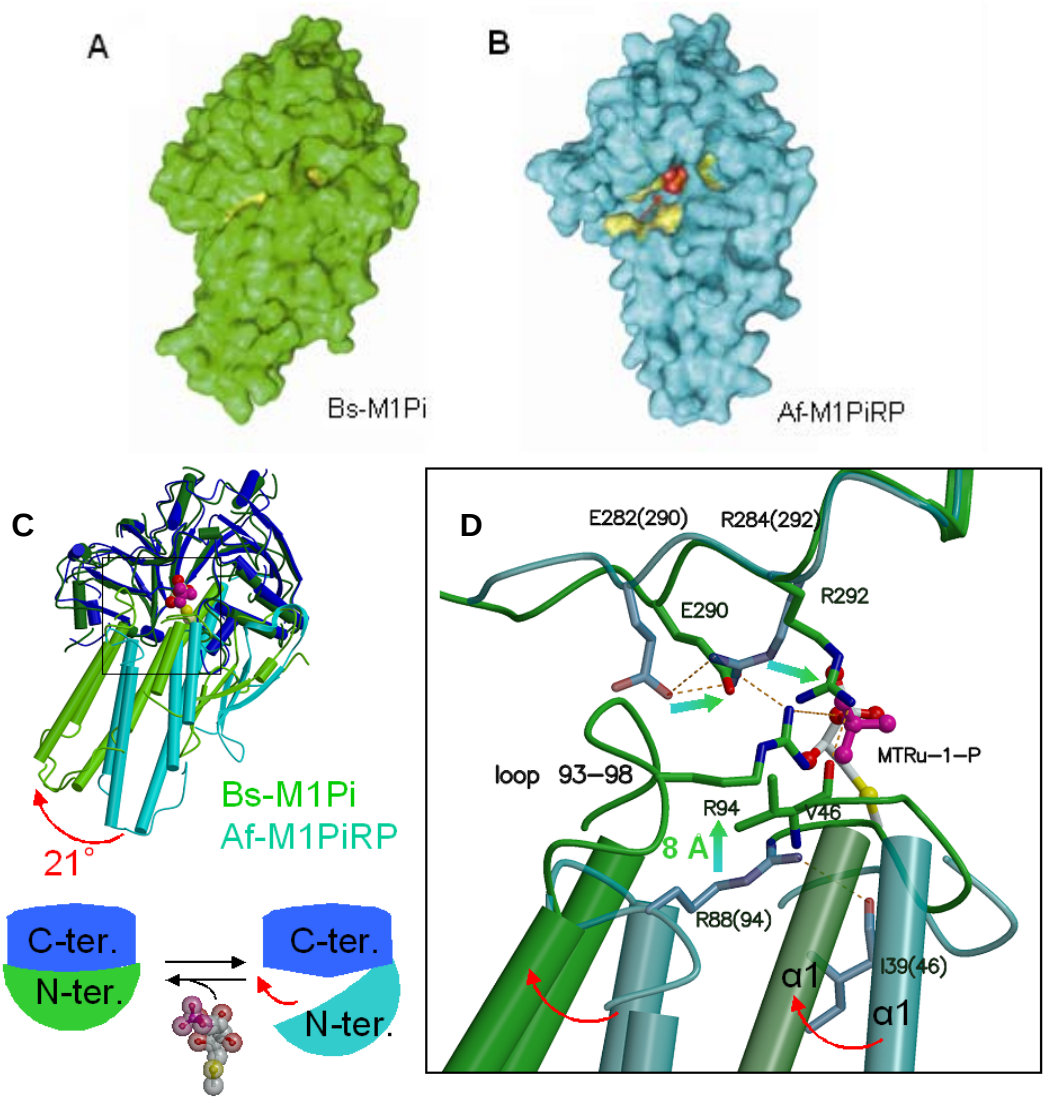

Figure 1-7 Structural comparison of Bs-M1Pi with Af-M1PiRP.
Molecular surfaces of Bs-M1Pi (A) and Af-M1PiRP (B) are shown in green and cyan. The residues involving MTRu-1-P recognition are colored in yellow. The arrow in (B) indicates the modeled MTRu-1-P, which suggest the opening of the catalytic site in the Af-M1PiRP structure. (C) Superposition of the C-terminal domain of Bs-M1Pi onto that of Af-M1PiRP; α-helices are shown in a cylinder representation. The N-terminal and the C-terminal domains of Bs-M1Pi are shown in light green and green, while those of Af-M1PiRP are shown in light blue and blue, respectively. (D) An enlarged view of the detailed hydrogen bond network. The color code is the same as (C). Dashed lines indicate hydrogen bonds.

1.4 Discussion

M1Pi belongs to the class of aldose-ketose isomerases, which catalyzes the isomerization of its cyclic substrate (7). In this case, the reaction mechanism can be proposed that involves the sugar ring opening followed by hydrogen transfer between C1 and C2 of the substrate.

Distinct from the substrates of other aldose-ketose isomerases (that normally possess hydroxyl groups on the cyclic C1), MTR-1-P has a phosphate group on the corresponding C1 position. Due to the electrophilicity of the phosphate group, the sugar ring of MTR-1-P would be much more chemically stable than the ordinary substrates possessing hydroxyl groups. The sugar ring opening of MTR-1-P probably requires an enzymatic mechanism. Aldose-ketose isomerase catalyzes the hydrogen transfer via two possible mechanisms: 1) enediol or 2) hydride transfer mechanisms (11). M1Pi possesses the hydride transfer mechanism in the absence of any divalent metal ions.

At the first step, the positively charged region composed of the side chains of Arg51, Arg94 and Lys251 participates in binding of the phosphate group of the substrate, forming a Michaelis complex. Simultaneously, a remarkable conformational change of the N- and C-terminal domains will be induced upon the substrate binding as described above, so that the pocket would be sequestered from the solvent region. In the second step, the sugar ring opening is catalyzed by donating a proton to the ring oxygen of the substrate MTR-1-P. As described above, the side chain of Asp240 is expected to play a role as either a donor or an acceptor (Fig. 1-8). Compared to xylose isomerase (XI) (43, 44), the side chain of Asp240 superimposes well on the catalytic water molecule of XI, which mediates proton transfer between O1 and O2 in XI. In the similar way, Asp240 would accept a proton from the O2 of MTR-1-P by the nucleophilic attack and donate a proton to the ring oxygen (in the MTR-1-P to MTRu-1-P direction) to promote the ring opening step of catalysis. Then, the deprotonated Cys160 probably stabilizes the positive charge generated

on C1. At the end of this step, the hydride on C2 transfers to C1 accompanying the electron flow from O2 toward C2 to form a carbonyl double bond and then yields the product MTRu-1-P (Fig. 1-9).

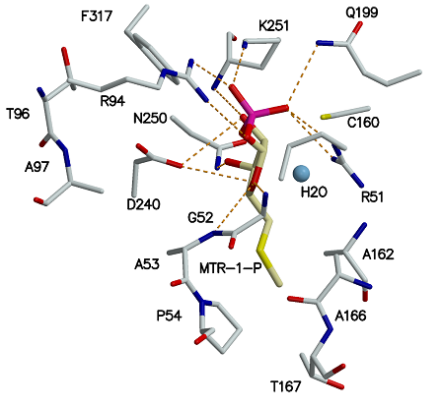

Figure 1-8 Substrate MTR-1-P binding model of Bs-M1Pi in the active site.
Hydrogen bonds are shown as orange dashed lines. Residues involved in the recognition of MTR-1-P are colored in white as sticks.

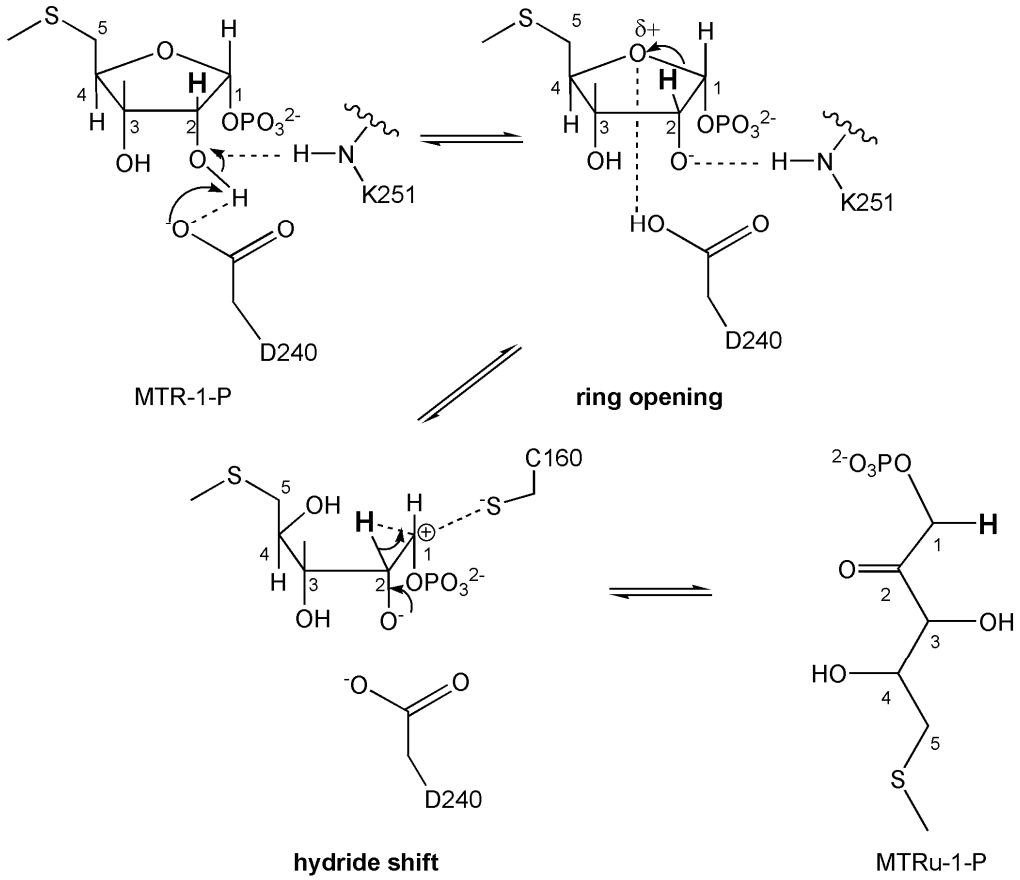

Figure 1-9 Proposed reaction mechanisms of M1Pi.
Proposed catalytic mechanism of the 1,2-hydride shift reaction of M1Pi based on the crystal structure of its product complex. The amino acid residues are shown in Bs-M1Pi numbering. D240 accepts a proton from the O2 of MTR-1-P by the nucleophilic attack and donates a proton to the ring oxygen of the substrate MTR-1-P. C1 is likely to become a carbocation intermediate.

Chapter II

Crystal structure of the apo form of 2,3-diketo-5-methylthiopentyl-1-phosphate enolase from *Bacillus subtilis*

2.1 Introduction

D-Ribulose-1,5-bisphosphate carboxylase/oxygenase (RuBisCO; EC 4.1.1.39) catalyzes the carboxylase reaction that fixes CO_2 on a five-carbon sugar phosphate, D-ribulose-1,5-bisphosphate (RuBP), to produce two molecules of 3-phosphoglycerate (3PGA) (Scheme 2-1A) (45, 46). RuBisCO is the key enzyme on the initial step of photosynthetic CO_2 assimilation in the Calvin cycle. Nevertheless, RuBisCO has two major enzymatic defects; the carboxylation reaction is extremely slow (k_{cat} = 3–4^{-1}) (47), and RuBisCO catalyzes an oxygenase reaction that fixes O_2 into RuBP, which competes with the carboxylase reaction (45, 46). Therefore, the photosynthetic CO_2 assimilation rate in plants can be limited by RuBisCO (48, 49). In order to overcome these disadvantages, plants manage to perform large amounts of RuBisCO protein. Indeed, RuBisCO protein constitutes ~50% of the soluble proteins in plant leaves and is the most abundant protein on the earth (50). To date, detailed discussions of several aspects of RuBisCO research are available; however, it has not yet contributed to create super RuBisCO with a high CO_2 fixation and a low O_2 affinity. Therefore, we have been interested in the molecular evolution of RuBisCO.

Based on the amino acid sequences and structures, RuBisCO is classified into three forms, referred to as Forms I, II, and III, and all RuBisCO in these groups catalyze both carboxylase and oxygenase reactions. Structures of Form I RuBisCOs have been extensively studied for various forms (Fig. 2-1): apo, decarbamylated form (E) (51, 52), carbamylated form complexed with Mg^{2+} (ECM) (53, 54), decarbamylated form complexed with PO_4^{3-}/SO_4^{2-} (E-PO_4^{3-}/SO_4^{2-}) (55-58), decarbamylated form complexed with RuBP/4CABP/XuBP (E-RuBP/4CABP/XuBP) (59-62), and

carbamylated form complexed with Mg^{2+} and RuBP/2CABP (ECM-RuBP/2CABP) (63-69). Two flexible loops, called loop-6 and 60's loop, have been observed to partition between "open" and "closed" conformations (55, 70, 71), that determine the solvent accessibility of the active site (72). Various RuBisCO structures have given at least three structural combinations of the two loops: both of loop-6 and 60's loop in open conformations observed in the E- and E-PO_4^{3-}/SO_4^{2-}-forms, both in closed conformations observed in the E-RuBP/4CABP/XuBP- and ECM-RuBP/2CABP-forms, and loop-6 in an open conformation and 60's loop in a closed conformation observed in the ECM-form. An exception has been found in the E-SO_4^{2-}-form of Form I RuBisCO from a red algae, *Galdieria partita*, which exhibits a high specificity for CO_2 fixation, adopts loop-6 in a closed conformation and 60's loop in an open conformation (58) .

Scheme 2-1 (A) Carboxylation reaction catalyzed by RuBisCO. (B) Enolization reaction catalyzed by 2,3-diketo-5-methylthiopentyl-1-phosphate enolase.

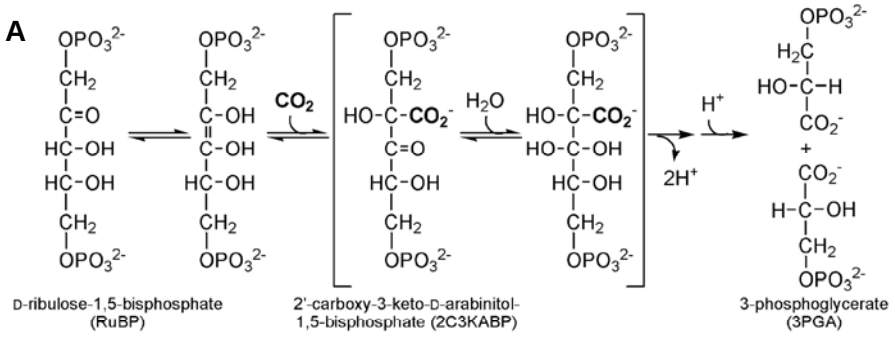

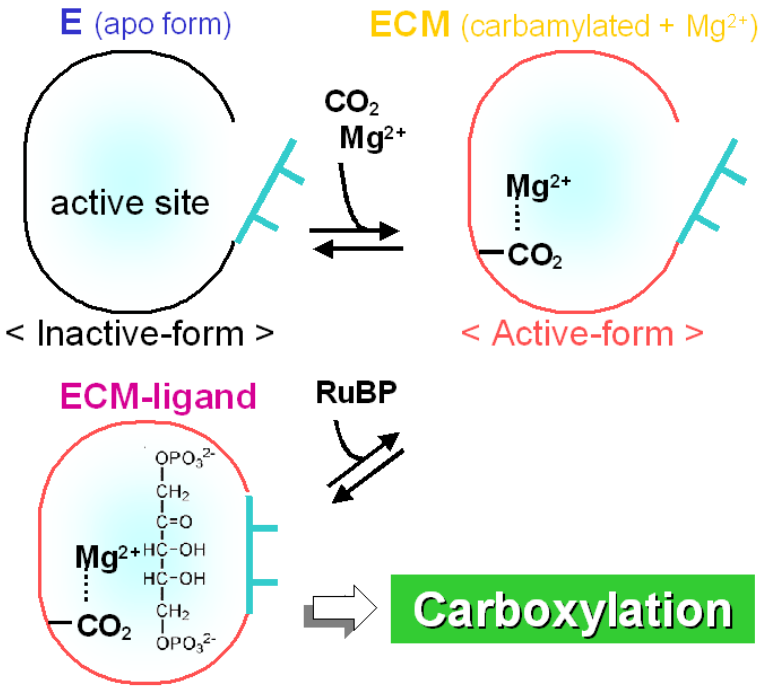

Figure 2-1 Activation mechanism of RuBisCO.

Many genome projects have revealed that proteins having homology to large subunits of RuBisCO may be present in bacteria, including *Bacillus subtilis* (73). These RuBisCO homologues are called RuBisCO-like proteins (RLPs), because they catalyze neither carboxylation nor oxygenation (7, 74, 75). Phylogenetic analysis indicates that RLPs may be further classified into at least three groups (RLP-α, β, and γ) (76, 77). More recently, the biological functions and structures of RLPs have become available. RLPs from *B. subtilis* (Bs), *Geobacillus kaustophilus* (Gk), and *Microcystis aeruginosa* (Ma), all of which belong to RLP-α, have been characterized as 2,3-diketo-5-methylthiopentyl-1-phosphate enolase (DK-MTP-1P enolase) (7, 10, 78). DK-MTP-1P enolase catalyzes enolization of 2,3-diketo-5-methylthiopentyl-1-phosphate （DK-MTP-1P）(Scheme 2-1B) and functions in the methionine salvage pathway, which salvages methionine from methylthioadenosine (79). Another RLP from *Rhodospirillum rubrum*, which also belongs to RLP-α, has been identified as 5-methylthio-D-ribulose-1-phosphate isomerase in a new, as-yet-uncharacterized, pathway for sulfur salvage (80). The molecular functions of the other RLPs

remain unknown, although the crystal structures have been solved for RLPs from *Chlorobium tepidum* and *Rhodopseudomonas palustris*, both of which belong to RLP-γ (81, 82).

Imker *et al*. have reported the crystal structures of four different forms of Gk-DK-MTP-1P enolase (60% sequence identity with Bs-DK-MTP-1P enolase) (10): PO_4^{3-}-bound decarbamylated form (E-PO_4^{3-}; PDB code: 2OEJ), carbamylated (activated) form complexed with Mg^{2+} (ECM; PDB code: 2OEK), carbamylated form complexed with Mg^{2+} and bicarbonate (ECM-HCO_3^-; PDB code: 2OEL), and carbamylated form complexed with Mg^{2+} and alternate substrate 2,3-diketohexane-1-phosphate (DK-H-1P) (ECM-substrate; PDB code: 2OEM). Based on these structural and biochemical studies (10), the enzyme is activated via carbamylation of Lys173 (equivalent to Lys201 in RuBisCO) at the active site and coordination with Mg^{2+}. DK-MTP-1P enolase is therefore considered to share the same activation mechanism as RuBisCO (83-87). Mutagenesis studies have demonstrated that Gk-DK-MTP-1P enolase utilizes the Nζ atom of Lys98 (Lys101 in *B. subtilis*) as a catalytic base to abstract the 1-*proS* proton on C1 of DK-MTP-1P (10). Because a residue equivalent to Lys98 is substituted by Asn in Forms I-III RuBisCO (see position 123 in Fig. 2-5), proton abstraction of DK-MTP-1P enolase is achieved by a different base from that of RuBisCO. As for the open-closed transition of loop-6 and 60's loop, the E-PO_4^{3-}-form of Gk-DK-MTP-1P enolase adopts both loop-6 and 60's loop in open conformations, while the other three forms (ECM, ECM-HCO_3^-, and ECM-substrate) adopt loop-6 in a closed and 60's loop in an open conformations. Whereas the structures of each form (E, ECM, and ECM-ligand) of RuBisCOs are available so far, the crystal structure of the apo, decarbamylated form (E) of DK-MTP-1P enolase remains unknown. If the structural information of the E-form of DK-MTP-1P enolase is available, dynamic events that occur in the discrete catalytic steps will be elucidated. In addition, the structure comparison with RuBisCO in the same enzymatic state allow to clarify structurally consistency in DK-MTP-1P enolase and RuBisCO, which may provide clues about

functional and evolutionary relationships between RLP and RuBisCO.

Here, we present the crystal structure of the E-form of Bs-DK-MTP-1P enolase. In the structure, the conformation of Lys150 (equivalent to Lys175 in RuBisCO) differs particularly from those of the other forms of Gk-DK-MTP-1P enolase. This unique conformational change is accompanied by changes in the φ and Ψ angles of Gly151, which is conserved in the sequences of Bs- and Gk- DK-MTP-1P enolases. Unlike the E-form of RuBisCO, in the E-form of DK-MTP-1P enolase, the loop at 299–311 (equivalent to loop-6 in RuBisCO), is in a closed conformation; and the loop at 37–46 (equivalent to 60's loop) is positioned about 15 Å apart from the active site. These structure features provide insights into potential functional alternations of RLP and RuBisCO.

2.2 Materials and Methods

2.2.1 Cloning and Expression of Bs-DK-MTP-1P enolase

The full-length DK-MTP-1P enolase *(mtnW)* gene was amplified from genomic DNA by PCR, which was performed with the following forward and reverse primers: 5'-GAGCTCTCATATGAGTGAGTGAGTTATTAG-3' and 5'-GCGGATCCTCATACGGCTT C-3'. Because of the presence of an *Nde*I site in *mtnW*, full-length *mtnW* was subcloned in pBC (Stratagene), and then digested partially with *Nde*I before a digestion with *Bam*HI. The fragments were ligated at *Nde*I/*Bam*HI site of pET15b (Novagen). The resulting recombinant protein consists of the DK-MTP-1P enolase sequence with extra 20 residues (MGSSHHHHHHSSGLVPRGSH) at the N-terminus containing the 6× His-tag and a thrombin cleavage site. *E. coli* strain BL21 (DE3) cells harbouring the DK-MTP-1P enolase expression plasmid were grown for 8 h in LB medium containing 50μg ml^{-1} ampicillin at 310 K. The cells were grown for a further 16 h at 303 K. The cells were then harvested by centrifugation at 6000*g* for 30 min. The cell pellet was resuspended in

buffer *A* (50 mM Na HEPES pH 7.4, 500 mM NaCl, 10mM Imidazole and 10 mM 2-mercaptoethanol) containing 1 mM PMSF, then disrupted by a French Press.

2.2.2 Purification

The disrupted cells were centrifuged at 400 000*g* at 277 K for 30 min. The supernatant was loaded onto a 5ml HiTrap Chelating column (GE Healthcare Biosciences) equilibrated with buffer *A*. The unbound proteins were flushed with buffer *A*. DK-MTP-1P enolase with the N-terminal histidine tag was eluted with a 215-300 mM imidazole gradient. Further purification to DK-MTP-1P enolase was carried out using a gel-filtration chromatography column (HiLoad 26/60 Superdex 200 prep grade, GE Healthcare Biosciences) equilibrated with buffer *B* (50 mM Na HEPES pH 7.4, 500 mM NaCl, 10 mM DTT, and 1 mM EDTA). Pooled fractions were concentrated to 10 mg ml^{-1} with Vivaspin 20 ml (10 kDa cutoff, Vivascience), and used for crystallization without removal of the N-terminal histidine tag. The protein concentration was determined by measuring the absorbance at 280 nm with a calculated molar absorption coefficient of 23 080 M^{-1} cm^{-1} (88). Recombinant DK-MTP-1P enolase from *B. subtilis* was successfully expressed and purified to homogeneity. The purity was checked by SDS-PAGE analysis (Fig.2-2).

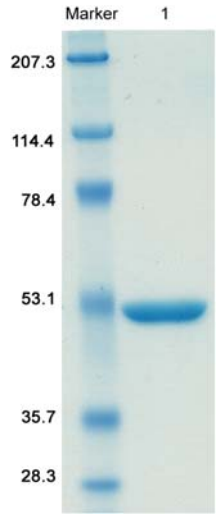

Figure 2-2 SDS-PAGE analysis of purified *B. subtilis* DK-MTP-1P enolase.
Maker, molecular weight markers (kDa). Lane 1, purified *B. subtilis* DK-MTP-1P enolase for crystallization.

2.2.3 Crystallization

The crystallization screen of 10 mg ml^{-1} DK-MTP-1P enolase in buffer *B* was initially performed with PEG/ion Screen (Hampton Research) by using the hanging-drop vapor diffusion method at 293 K. The drop size was 2μl, with protein, reservoir solution ratio of 1:1. Crystals with maximum size of 0.1 × 0.05 × 0.05 mm were obtained using PEG/ion Screen condition No.13 [200 mM Sodium Thiocyanate, 20% (w/v) PEG3350] within a week. To refine the conditions, we varied the pH and concentrations of protein, salt, or precipitant. Optimized crystallization was performed with the hanging-drop vapor-diffusion method at 293 K with the following: a drop (2μl) containing equal volumes of protein (10 mg ml^{-1} DK-MTP-1P enolase) and reservoir solution [140 mM Sodium Thiocyanate, 21% (w/v) PEG3350] suspended over 300μl reservoir solution. Crystals suitable for diffraction appeared after five days (Fig. 2-3).

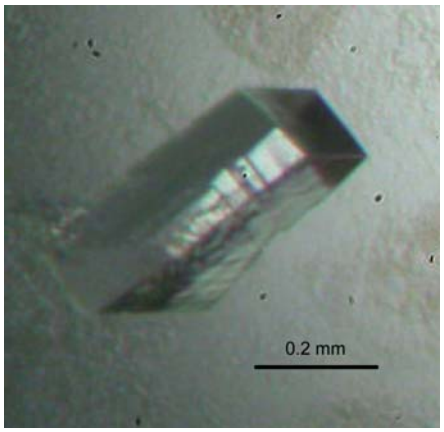

Figure 2-3 Crystal of *B. subtilis* DK-MTP-1P enolase. (Maximum size: 0.1 × 0.15 × 0.3 mm.)

2.2.4 X-ray data collection

The crystals were soaked for a few seconds in reservoir solution containing 10% (v/v) glycerol. Flash-cooled crystals were then mounted into the nitrogen stream at 100 K. The X-ray diffraction data were collected to 2.3 Å resolution on a DIP-6040 detector (Bruker-AXS) using synchrotron radiation of wavelength 1.0 Å at the BL44XU beamline in SPring-8 (Fig. 2-4). Data collection was performed with a total oscillation range of 220°, with a step size of 1.0° and an exposure time

of 10 sec per frame. Crystals belonged to the space group $P2_1$ based on the systematic absences, with the cell parameters a = 79.3, b = 91.5, c = 107.0, β = 90.8. The crystallographic and X-ray data statistics are summarized in Table 2-1. The value of the Matthews coefficient is 2.2 $Å^3$ Da^{-1} for the four monomers in the asymmetric unit, corresponding to a solvent content of 43%, a typical value for protein crystals (89). The self-rotation function at χ = 180° was calculated in the 15-3.5 Å resolution range with an integration radius of 40 Å (*POLARRFN*; (90)). The result indicates the existence of pseudo orthorhombic symmetry at (θ φ χ) = (90.3, 180, 180°) and (0.3, 180, 180°). The peak intensity with respect to the crystallographic axis was 64.4%. All diffraction data were processed using the MOSFLM program (91) and the *CCP*4 program suite (90).

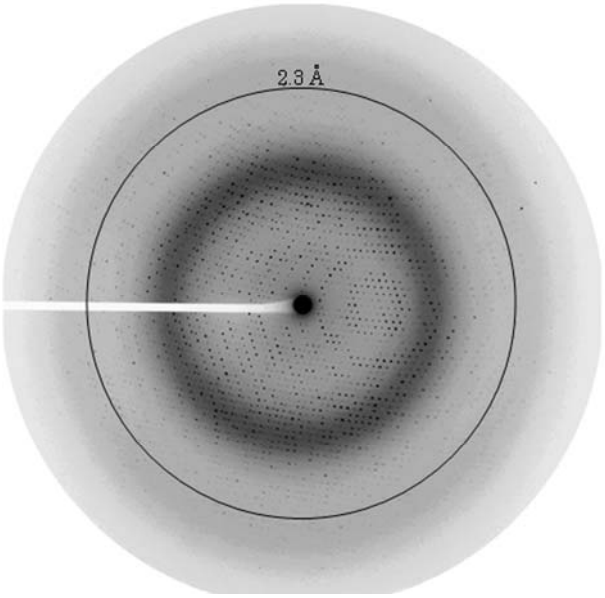

Figure 2-4 X-ray diffraction image from a *B. subtilis* DK-MTP-1P enolase crystal.

2.2.5 Structure determination and Refinement

Structure determination was performed by molecular replacement using *MOLREP* v.7.3 (92) from the *CCP*4 v.6.0 software suite (90). A dimer of DK-MTP-1P enolase structure of *G. kaustophilus* (PDB code: 2OEK) was used as a search model. The results of molecular replacement suggest these crystals contain two independent dimers per asymmetric unit. Refinement procedures for

Bs-DK-MTP-1P enolase was carried out using the program CNS (29) without non-crystallographic symmetry (NCS) restrains/constraints. The structures were visualized and modified using the programs O (Alwyn Jones, Uppsala University, Sweden), and COOT (30). The final R_{work} and R_{free} are 20.1 and 24.2% for the E-from of Bs-DK-MTP-1P enolase at 2.3 Å resolution. The electron density map was clear for almost the entire polypeptide of Bs-DK-MTP-1P enolase. The stereochemical qualities of the final structures were assessed with programs PROCHECK (31). Figures were generated by MOLSCRIPT (33) and RASTER3D (34) , and all structural comparisons were carried out using the program LSQKAB (90).

Table 2-1 Date collection and refinement statistics
Values in parentheses are for the highest resolution shell (2.42 -2.30 Å)

	The apo, decarbamylated form
Beamline	SPring-8 BL44XU
Space group	$P2_1$
Unit-cell parameters (Å, ˚)	a = 79.3, b = 91.5, c = 107.0, β = 90.8
Resolution range (Å)	30.5 - 2.30
No. of molecules per asymmetric unit	4
V_M (Å^3/dalton)	2.2
V_{solv} (%)	43
No. of measured reflections	259,484
No. of unique reflections	64,719
$I/\sigma(I)$	7.2 (2.4)
R_{merge} (%)$^+$	8.4 (27.3)
Completeness (%)	95.0 (95.3)
R_{work} (%)	20.1
R_{free} (%)	24.2
Rms deviations	
Bonds (Å)	0.006
Angles (˚)	1.4
Ramachandran statistics, residues in	
Most facvoured region (%)	88.1
Additionally allowed region (%)	11.3
Generally allowed region (%)	0.6
Disallowed region (%)	0.0

$^+$ Rmerge = $\Sigma|I(k)-I|/\Sigma I(k)$, where $I(k)$ is value of the kth measurement of the intensity of a reflection, I is the mean value of the intensity of that reflection and the summation is the over all measurements.

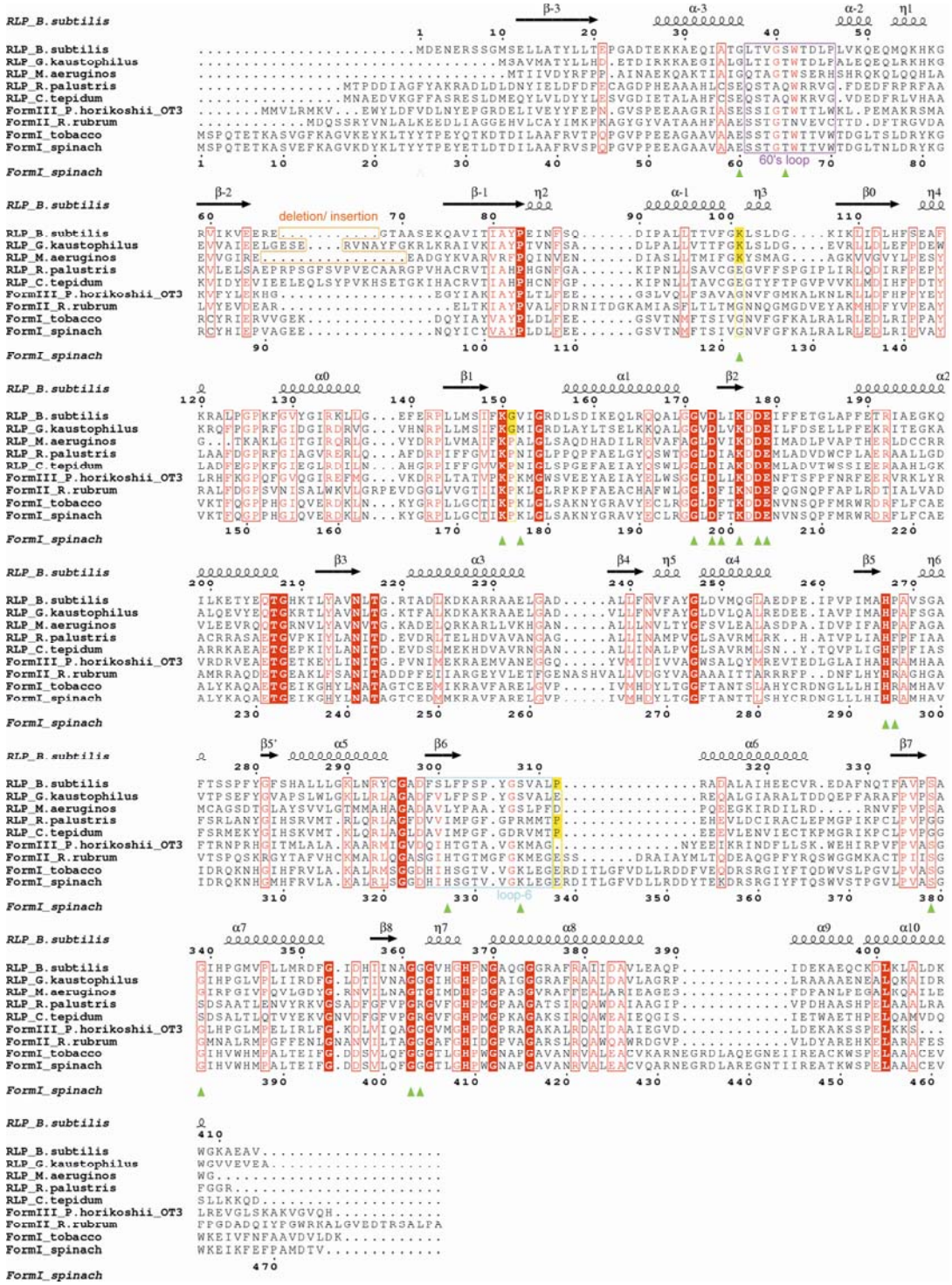

Figure 2-5 Sequence alignment of *Bacillus subtilis* DK-MTP-1P enolase and homologous proteins. The sequences are five RLPs of *B. subtilis* (NP_389242), *Geobacillus kaustophilus* (YP_146806), *Microcystis aeruginosa* PCC 7806 (CAJ43366), *Rhodopseudomonas palustris* (NP_947514) and *Chlorobium tepidum* (NP_662651) and four RuBisCOs of *Pyrococcus horikoshii* OT3 (Form III; NP_142861.1)*, Rhodospirillum rubrum* (Form II; YP_427487), tobacco (Form I; NP_054507), and spinach (Form I; NP_054944). Numbers above the sequences as well as the secondary structure assignments refer to those of Bs-DK-MTP-1P enolase. The secondary structures of α-helices, β-strands and 3_{10}-helices are denoted by the Greek characters, α, β and η, respectively. The fully conserved residues are highlighted in red boxes and the red amino acid residues are moderately conserved. The deletion region between β-2 and β-1 is highlighted with an orange box. 60's loop and loop-6 are highlighted in magenta and cyan boxes, respectively. Numbers below the sequences refer to those of spinach RuBisCO and are used as a general position. The residues involved in the substrate binding and catalytic activity of RuBisCO are marked by green triangles. In Bs-DK-MTP-1P enolase, some key residues described in the text, are highlighted in yellow.

2.3 Results and Discussion

2.3.1 Overall structure

The final model of the apo, decarbamylated form (E) of Bs-DK-MTP-1P enolase contains two dimers in the asymmetric unit of the crystal (residues 11–410 except for 23–24 and 67–69 for chain A, residues 11–66 and 72–411 for chain B, residues 11–39, 48–66, and 73–409 for chain C, residues 11–36, 46–67, and 73–413 for chain D, Fig. 2-6A). Each polypeptide can be superimposed with an rms deviation of 0.48 to 0.97 Å for their Cα atoms. The alternative structures of individual polypeptides arise from differences in the crystal-packing environment. The structure of Bs-DK-MTP-1P enolase resembles those of four forms of Gk-DK-MTP-1P enolase (rms deviation of 0.59 to 0.87 Å), except for the insertion of an N-terminus (residues 1–9), a deletion between residues 65–72 (Figs. 2-5, 2-6B and 2-7A), and a few residues at the active site, as we discuss below. These insertions and deletions are between secondary structure elements and are presumably not implicated in catalysis. In analogy with Gk-DK-MTP-1P enolase, the active sites are located at the interface between a C-terminus of $(\beta/\alpha)_8$-barrel and an N-terminal domain of the neighboring subunit within the dimer (2-6A). The active site is composed of a glycine-rich region for a phosphate binding (Gly339, Gly362, and Gly363), a positively charged residue (His267) and hydrophobic residues (Pro268 and Leu301), which are also structurally conserved in Gk-DK-MTP-1P enolase (10).

2.3.2 Structural comparison with homologous proteins

In the same order as the sequence conservations, the structure of Bs-DK-MTP-1P enolase most closely resembles those of the other groups' RLPs (25~60% sequence identity) and Form III RuBisCOs (~30% sequence identity), and resembles those of Form I (~23% sequence identity) and Form II (~23% sequence identity) RuBisCOs to some degree (Fig. 2-9). E-form RLPs from *C.*

tepidum (PDB code: 1YKW) and *R. palustris* (PDB code: 2QYG), both of which belong to RLP-γ, can be superimposed with rmsd of 2.2 and 2.3 Å for their 367 and 378 Cα atoms, except for their insertions at the N-terminus and the loop between β-2 and β-1. The rmsd between Bs-DK-MTP-1P enolase and two forms (E; PDB code: 2CWX and E-SO_4^{2-}; PDB code: 2D69) of Form III RuBisCO from *Pyrococcus horikoshii* OT3 are both 2.3 Å for their 380 Cα atoms (Fig. 2-7B). The rmsd between Bs-DK-MTP-1P enolase and three forms (E; PDB code: 1RLD, ECM; PDB code: 1AUS, and ECM-2CABP; PDB code: 8RUC) of Form I RuBisCO from tobacco or spinach are 2.7 to 3.0 Å for their 377 Cα atoms (Fig. 2-7D); the rmsd between Bs-DK-MTP-1P enolase and three forms (E; PDB code: 5RUB, ECM; PDB code: 2RUS and ECM-RuBP; PDB code: 9RUB) of Form II RuBisCO from R. rubrum are 3.3 to 3.5 Å for their 352 Cα atoms (Fig. 2-7C).

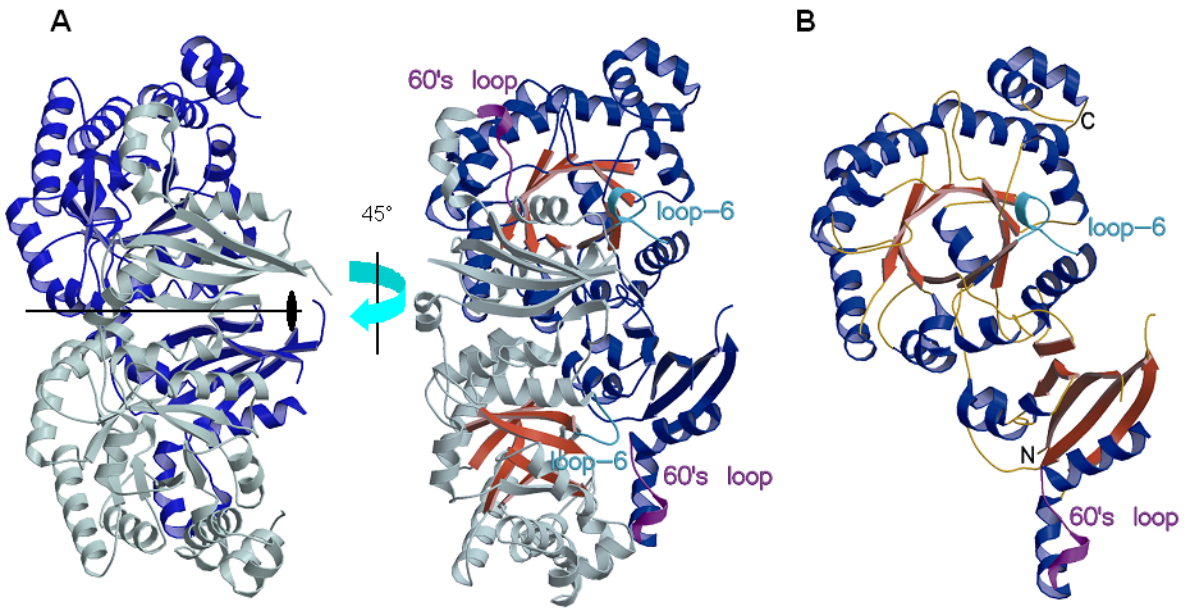

Figure 2-6 Structural comparison of DK-MTP-1P enolase
(A) Dimer structure of Bs-DK-MTP-1P enolase. Each monomer is colored in blue and gray, respectively. (B) Monomer structure of Bs-DK-MTP-1P enolase. The monomer can be divided into two domains: an N-terminal domain (residues 1-143) and a C-terminal $(\beta/\alpha)_8$-barrel domain (residues 144-414), respectively. Loop-6 and 60's loop are colored in cyan and magenta, respectively.

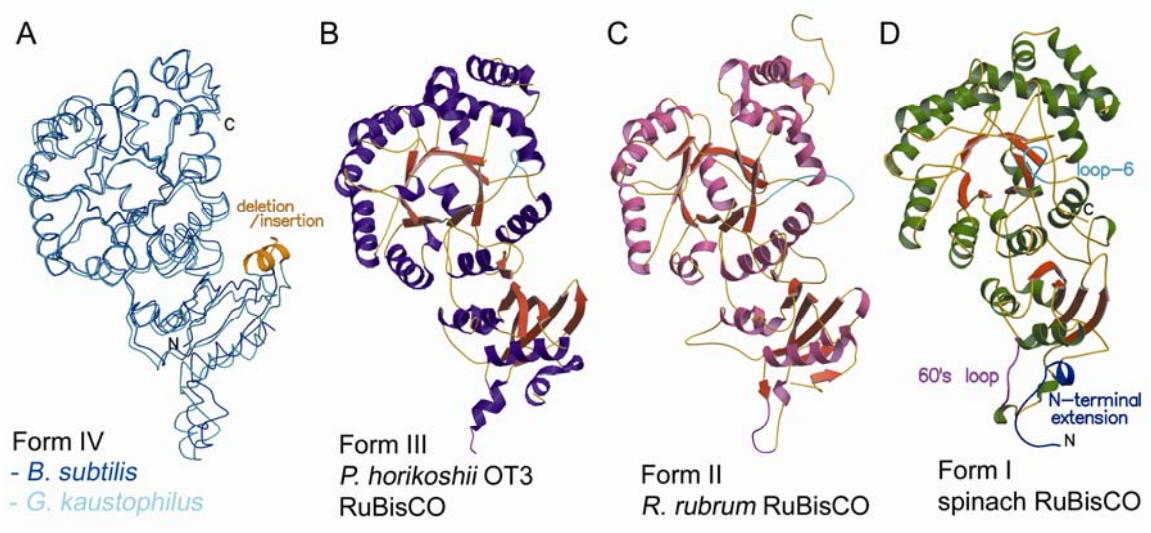

Figure 2-7 Structural comparisons of DK-MTP-1P enolase and RuBisCO.
(A) Superposition of the α-carbon backbones of Bs- (blue) and Gk- (dark cyan; PDB code: 2OEM) DK-MTP-1P enolases (Form IV). The deletion or insertion region is shown as a cartoon diagram. Monomer structures of RuBisCO from *P. horikoshii* OT3 (B; Form III), and *R. rubrum* (C; Form II). (D) Monomer structure of RuBisCO from spinach (PDB code: 8RUC) (Form I). An N-terminal extension, which lacks in DK-MTP-1P enolase, is colored in blue. Loop-6 and 60's loop are colored in cyan and magenta, respectively.

2.3.3 Induced fit of Lys150 to the active site

In DK-MTP-1P enolase, the substrate binding appears to undergo an induced fit of Lys150 at the active site. Lys150 (at position 175 in Fig. 2-5) is completely conserved among Forms I-III of RuBisCOs and RLPs, and is a key residue to participate in binding to the 1-phosphate group of the substrate during catalysis (Figs. 2-8A and 2-8B). The side chains of Lys150 exhibit a disordered conformation in chains B and C, but they are ordered in chains A and D, pointing toward a water molecule in the solvent region (Fig.s 2-8C and 2-8D). In the latter case, both the main chain N atom of Lys150 and the main chain O atom of Gly151 form hydrogen bonds with the side chain of Gln163 (Table 2-2). It undergoes a flip of the main chain carbonyl group of Lys150, thus giving an opposite orientation of the Lys150 side chain to the active site (Figs. 2-8A and 2-8C). Upon this conformational change, the active site prior to substrate binding becomes solvent accessible.

Meanwhile, in the ECM-, ECM-HCO_3^--, and ECM-substrate-forms of Gk-DK-MTP-1P enolase, both of the main chain N and C atoms of Lys147 (Lys150 in *B. subtilis*) form

water-mediated hydrogen bonds to the side chain of Glu160 (Gln163 in *B. subtilis*), resulting in the side chain of Lys147 lying inside the active site (Fig. 2-8A and Table 2-2). This conformational change of Lys150 side chain, depending on the enzymatic states, is induced by changes in the φ (-153 to +58 degrees) and Ψ (+67 to +38 degree) angles of Gly151 (at position 176 in Fig. 2-5). Because this Gly is conserved in Bs- and Gk-DK-MTP-1P enolases (but not in Ma-DK-MTP-1P enolase), the conformational change might be the common event in Bs- and Gk-DK-MTP-1P enolases.

Such a dynamic conformational change of Lys175 (Lys150 in *B. subtilis*) has never been observed in the structures of various forms of RuBisCOs (Fig. 2-8B). One reason for this different behavior of RuBisCO may come from Pro176 conserved in RuBisCOs (at the same position as Gly151 in *B. subtilis*). Pro must impose the rigid constraints on its φ and Ψ angles; indeed, the two angles of Pro176 are virtually invariant (φ (-74 to -64 degrees) and Ψ (+151 to +158 degrees)) in the distinct states of RuBisCOs. Another reason could be highly conserved Thr71 (or Ser71) at the carboxyl end of 60's loop in RuBisCOs. In RuBisCOs from spinach and tobacco, the side chain of Thr71 interacts with carbonyl group of Lys175, which must stabilize the conformation of Lys175 (Table 2-2). Such an interaction is not observed in DK-MTP-1P enolase, because DK-MTP-1P enolase lacks the same Thr (or Ser) and the loop at 37–46 (equivalent to 60's loop in RuBisCO) is located 15 Å apart from the active site. Exceptions are found in some Form III RuBisCOs, which do not conserve the Thr or Ser at the position 71 (e.g. *P. horikoshii* RuBisCO). However, in that case, Lys175 is sandwiched between Pro174 and Pro176, both of which are conserved in their sequences (e.g. *P. horikoshii*, see position 174 and 176 in Fig.2-5). The two Pro residues perhaps contribute to the conformational rigidity of Lys175. Thus, the difference on the primary and tertiary structures between RLP and RuBisCO is likely to affect the structural property of Lys175, which may reflect the functional alternation of RLP and RuBisCO.

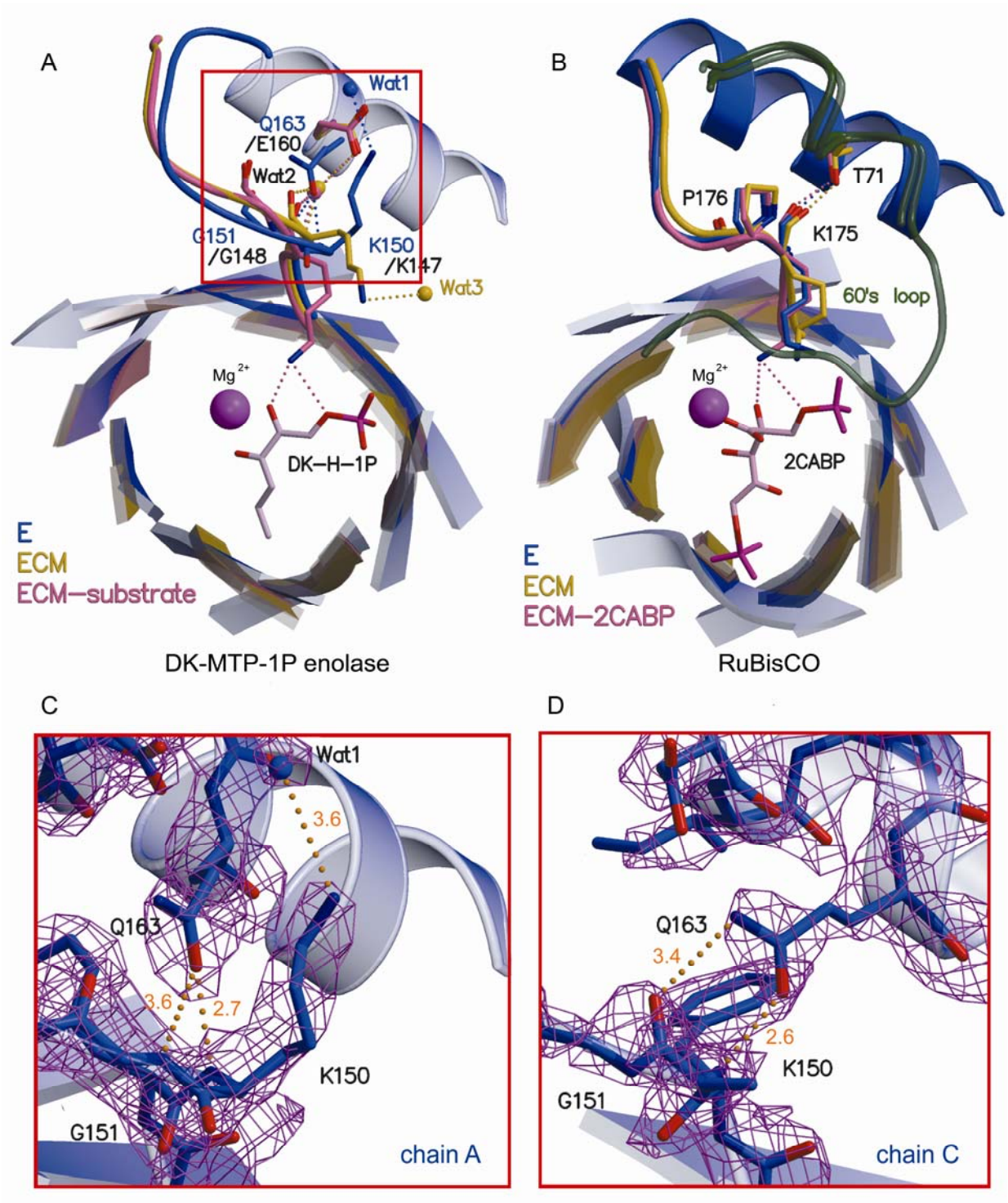

Figure 2-8 Active site structures of DK-MTP-1P enolase and RuBisCO.
(A) The inactivated form (E) of Bs-DK-MTP-1P enolase is colored in blue. The activated unliganded form (ECM) of Gk-DK-MTP-1P enolase (PDB code: 2OEK) is in yellow and it is bound to the alternate substrate 2, 3-diketohexane-1-phosphate (DK-H-1P) (ECM-substrate; PDB code: 2OEM) that is in magenta. The structures are superimposed via their $(\beta/\alpha)_8$-barrel domains. The side chains of residues involved in conformational change are shown as stick, with oxygen in red and nitrogen in dark blue. The water molecules, which is involved in the conformational change of Lys150 (Lys147 in *G. kaustophilus*) are shown as CPK in the same color as each form. Hydrogen bonds are shown as dashed lines and colored as well as each form. (B) The E-form of tobacco RuBisCO (PDB code: 1RLD) is colored in blue. The ECM-form of spinach RuBisCO (PDB code: 1AUS) is in yellow, and it is bound to transition state analogue 2-carbox-D-arabinitol-1,5-bisphosphate (2CABP) (ECM-2CABP; PDB code: 8RUC) that is in magenta. 60's loops from the opposite monomers are shown as green line representations. The ligands and residues are colored in the same as in (A). Enlarged view and the electron density around Lys150 for chains A (C) and C (S). The *Fo-Fc* omit maps of Lys150 is countered at 2.5σ level (colored in magenta). Hydrogen bonds are shown as orange dashed lines with the lengths indicated [Å].

Table 2-2 Hydrogen bonds involved in Lys150 (Lys175 in RuBisCO)

	DK-MTP-1P enolase			RuBisCO		
Active state	Interacting atoms		Distance (Å)	Interacting atoms		Distance (Å)
E	Lys150 N	Gln163 $O^{\varepsilon 1}$	2.7	Lys175 O	Thr71 O	2.6
	N^{ζ}	Water1	3.6			
ECM	Lys147 (150) N	Water2	2.7	Lys175 O	Thr71 $O^{\gamma 1}$	2.4
	O	Water2	3.1			
	N^{ζ}	Water3	3.5			
ECM-ligand	Lys147 (150) N	Water2	3.1	Lys175 O	Thr71 $O^{\gamma 1}$	2.6
	O	Water2	2.9	N^{ζ}	CABP O1	3.4
	N^{ζ}	Substrate O1	3.3		CABP O2	3.2
		Substrate O2	2.9			

2.3.4 Open/closed conformational changes of loop-6 and 60's loop

As described above, RuBisCO adopts an open or a closed conformation accompanied by large structural change of loop-6 and 60's loop. Although DK-MTP-1P enolases have the equivalent two loops, the strong correlations between the conformations of two loops and the activation or binding states are not seen in Bs- and Gk-DK-MTP-1P enolases. Loop-6 and 60's loop of the E-PO_4^{3-}-form of Gk-DK-MTP-1P enolase are both in open conformations, while the E-form of Bs-DK-MTP-1P enolase, and the ECM-, ECM-HCO_3^--, ECM-substrate-forms of Gk-DK-MTP-1P enolase adopt loop-6 in an open conformation and 60's loop in a closed conformation (Fig. 2-9A). However, if we focus on available crystal structures of other RLPs, a rule for loop-6 conformation can be found between primary and tertiary structures. The RLP structures of *B. subtilis*, *C. tepidum*, and *R.*

palustris, all of which have been solved as E-forms, show loop-6 in a closed conformation. And all three proteins conserve Pro at position 338 in Fig. 2-5, which is located at the carboxyl end of loop-6 (Fig. 2-9B). On the other hand, the corresponding residue is substituted with Glu in Gk-DK-MTP-1P enolase and loop-6 of the E-PO_4^{3-}-form of Gk-DK-MTP-1P enolase is in a disordered open conformation. These observations suggest that rigid constraints on the φ and Ψ angles on Pro at position 338 may stabilize loop-6 in a closed conformation, in the absence of any ligands. In Bs-DK-MTP-1P enolase, the interactions involved in two residues (Tyr306 and Arg313) on loop-6 and two residues (Arg350 and Asp351) on a neighboring helix (α7) also support to stabilize the closed conformation of loop-6 (Fig. 2-9B); however, these residues are not primary and structurally conserved in the other RLPs. Therefore, Bs-DK-MTP-1P enolase may have a tendency to adopt loop-6 in a closed conformation; this tendency is probably not common in the other DK-MTP-1P enolases, although several RLPs that conserve the residue Pro at position 338 may have.

Unlike RuBisCO, loop at 37–46, equivalent to 60's loop (residues 61–70 in RuBisCO), is positioned about 15 Å apart from the active site in Bs- and Gk-DK-MTP-1P enolases (Figs. 2-9A and 2-9C). This tendency can be seen in all structurally available RLPs. The primary structure of loop at 37-46 is less conserved within RLPs, and the conformation of loop 37–46 is mainly stabilized by the main chain hydrogen bonds (Fig. 2-9C and Table 2-3). Therefore, the unique conformation of 60's loop in RLPs is not caused by RLP-specific amino acid residues on the loop at 37-46. On the other hand, in RuBisCO, 60's loop is partially disordered in the E-form and then becomes an ordered, closed conformation in the ECM- and ECM-ligand-forms (Fig. 2-9C). The ordered conformation of 60's loop is stabilized by an N-terminal extension (at position 1–24 in Fig. 2-5) of RuBisCO, where seven amino acid residues (Phe13, Lys14, Gly16, Val17, Lys18, Tyr20, and Tyr24) participate in the tight interaction with 60's loop. Meanwhile, DK-MTP-1P enolases

lack the corresponding N-terminal domain (Figs. 2-5, 2-6B, and 2-7D). Thus, a lack of N-terminal domain may be one reason for the invariant structure of loop at 37–46 in DK-MTP-1P enolase.

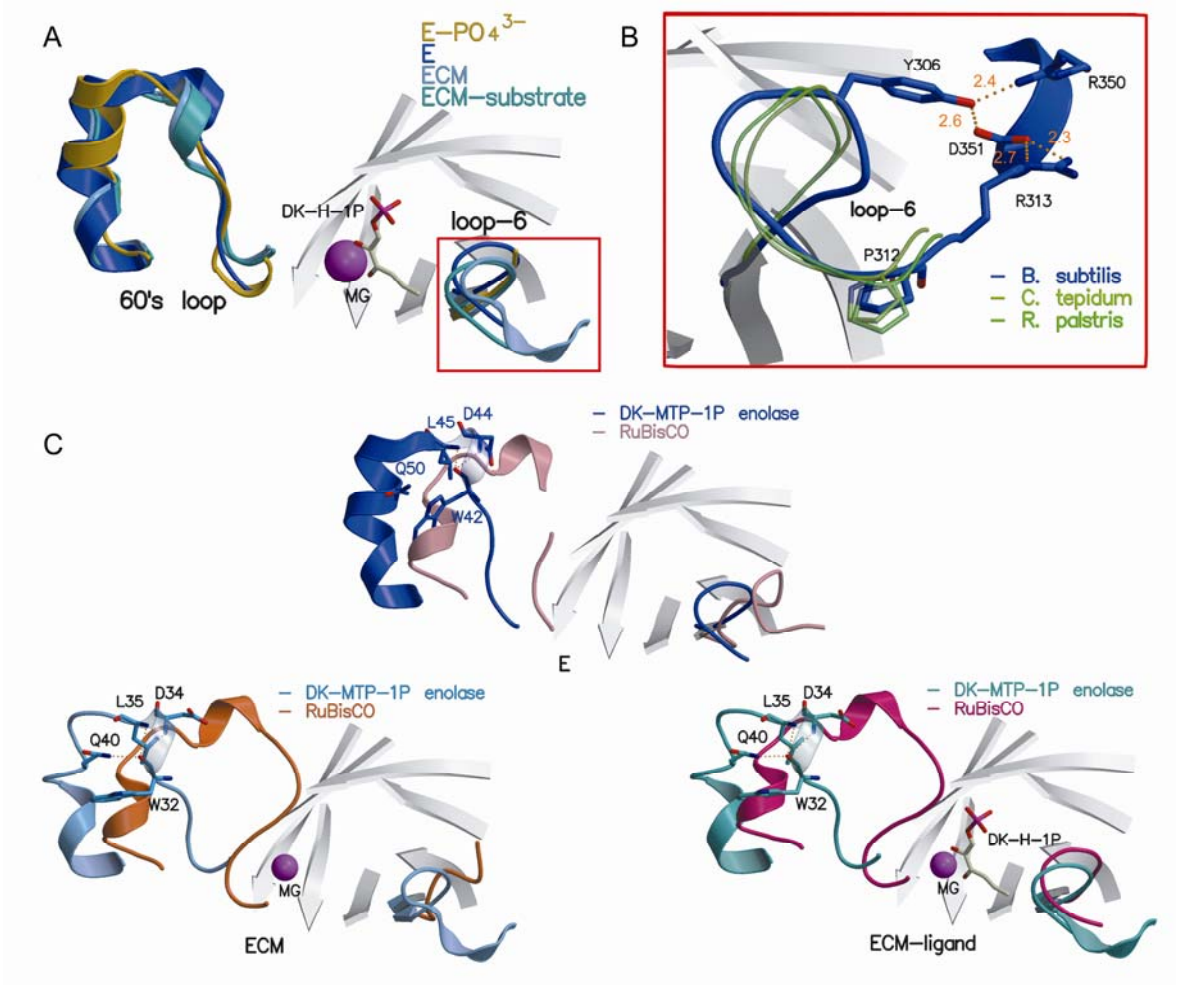

Figure 2-9 Structural comparison of the two loops equivalent to loop-6 and 60's loop in DK-MTP-1P enolase and RuBisCO

(A) The E-form of Bs-DK-MTP-1P enolase is colored in blue and the E-PO_4^{3-}-form of Gk-DK-MTP-1P enolase (PDB code: 2OEJ) is in yellow. The ECM-form of Gk-DK-MTP-1P enolase (PDB code: 2OEK) is colored in skyblue, and it is bound to 2,3-diketohexane-1-phosphate (DK-H-1P) (ECM-substrate; PDB code: 2OEM) that is in dark cyan. (B) Enlarged view of loop-6 in Bs-DK-MTP-1P enolase and superpositions of loop-6 with *C. tepidum* and *R. palustris*. The side chains of those residues involved in hydrogen bonds or structural stabilization are shown as sticks with oxygen in red and nitrogen in dark blue. Hydrogen bonds are shown as orange dashed lines with the lengths indicated [Å]. (C) Superposition of each form's DK-MTP-1P enolase and RuBisCO. Bs- and Gk-DK-MTP-1P enolases are in the same colors as in (A). The E-form of tobacco RuBisCO (PDB code: 1RLD) is shown in pink. The ECM-form of spinach RuBisCO (PDB code: 1AUS) is in orange, and it is bound to 2CABP (ECM-2CABP; PDB code: 8RUC) that is in red. The side chains of those residues involved in hydrogen bonds on 60's loop of DK-MTP-1P enolase are represented as sticks. The color coding is the same as in (B).

Table 2-3 Hydrogen bonds on 60's loop in DK-MTP-1P enolase

Active state	Interacting atoms		Distance (Å)
E	Trp42 O	Ala44 N	3.1
		Leu45 N	3.4
ECM	Trp32 (42) O	Ala34 (44) N	3.1
		Leu35 (45) N	3.0
		Gln40 (50) $N^{\varepsilon 2}$	3.2
ECM-ligand	Trp32 (42) O	Ala34 (44) N	3.2
		Leu35 (45) N	3.1
		Gln40 (50) $N^{\varepsilon 2}$	3.2

2.4.5 Structural comparison of loop-6 with a high CO_2 fixation RuBisCO

The gaseous CO_2 and O_2 are the competitive substrates in RuBisCO, the activity of which is characterized by the specificity factor, $S_{C/O}$ (= $V_C K_O / V_O K_C$, where V_C, V_O and K_C, K_O are the V_{max} and K_m values for CO_2 and O_2, respectively). A thermophilic red alga, RuBisCO from *Galdieria partita* has the highest $S_{C/O}$ (238 at 25˚C) among the RuBisCOs reported so far (93). Unlike other RuBisCO structures, loop-6 in the closed conformation has been observed in the E-SO_4^{2-}-form of *Galdieria* RuBisCO (58). Thus, a tendency to stabilize loop-6 in the closed state may be related to the efficient CO_2 fixation of RuBisCO. Structural comparison of loop-6 between Bs-DK-MTP-1P enolase and *Galdieria* RuBisCO revealed their structurally common stabilization. *Galdieria* RuBisCO has Pro339 at the carboxyl end of loop-6, which corresponds to the next residue of Pro312 in Bs-DK-MTP-1P enolase. The main chain carbonyl oxygen of Val332 (corresponds to Tyr306 in Bs-DK-MTP-1P enolase) forms a hydrogen bond with the side chain of Gln386 on α-7 helix (Fig. 2-10). In RuBisCO structures, loop-6 appears to undergo the transition from the open to

the closed state by the changes in the φ and ψ angles of residues Val332 and Glu338 (Tyr306 and Pro312 in Bs-DK-MTP-1P enolase, respectively). Therefore, similarly positioned Pro (at the position 338 or 339 in Fig. 2-5) and hydrogen bonds between loop-6 and α-7 helix seems to stabilize loop-6 in the closed conformation.

In future work, the enzymatic activities of RuBisCO need to be measured in order to examine the effects of site-specific mutations, which have Pro at the position 338 or 339, or hydrogen bond network between loop-6 and α-7 helix. Additionally, the detailed X-ray structural analysis for these mutated enzymes will be required to explain how the stabilization of loop-6 in the closed state affects a high CO_2 fixation. Based on these results, the creation of super RuBisCO with much higher $S_{C/O}$, will take a new turn to realize the sustainable development on the earth.

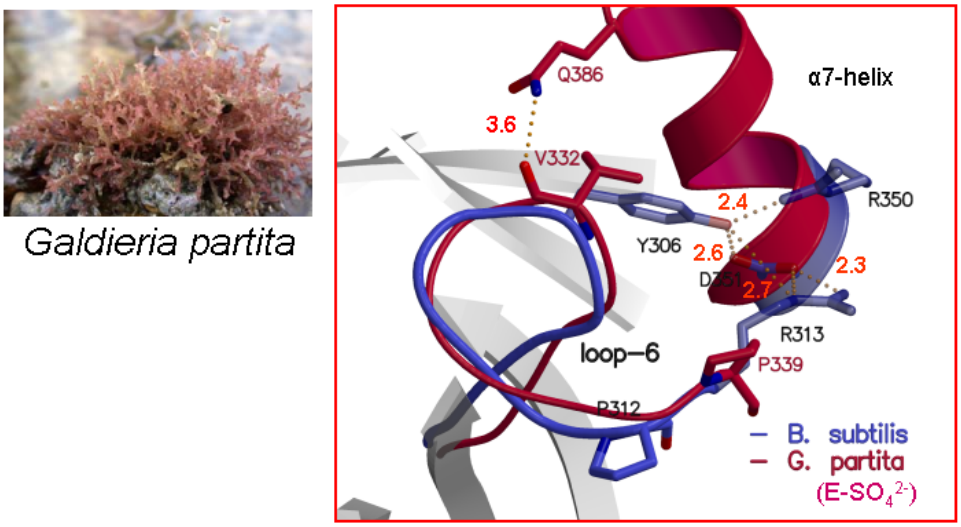

Figure 2-10 Structural comparison of loop-6
Enlarged view of superpositioned loop-6 in Bs-DK-MTP-1P enolase (colored in blue) and *G. partita* RuBisCO (colored in red). The side chains of those residues involved in hydrogen bonds or structural stabilization are shown as sticks with oxygen in red and nitrogen in dark blue. Hydrogen bonds are shown as orange dashed lines with the lengths indicated [Å].

Conclusion

The study was undertaken for obtaining insight into structure-function relationship on enzymes of the methionine salvage pathway in *Bacillus subtilis*. Here the structural analyses of two enzymes (M1Pi and DK-MTP-1P enolase) are reported. Structural comparison with homologous proteins revealed the reaction mechanism and characteristic structural features to explain their functions in detail. These results would contribute to the knowledge of new reaction schemes and applications for higher CO_2-fixation to establish a sustainable development on the earth.

In Chapter I, the purification and preliminary crystallographic studies of *B. subtilis* M1Pi (Bs-M1Pi) are reported. Additionally, the crystal structures of Bs-M1Pi in complex with its product MTRu-1-P, or a sulfate have been determined at 2.4 and 2.7 Å resolution, respectively. The electron density clearly shows the presence of each compound in the active site. Several high resolution crystal structures have become available for M1Pi homologous proteins in the Protein Data Bank. Although yeast Ypr118w has been characterized as M1Pi, three M1Pi-related proteins of *T. maritima*, *P. horikoshii* OT3 and *A. fulgidus* have been annotated as putative proteins of unknown function. The structural comparison with these homologous proteins enables to predict their functions and to explain how the substrate uptake of Bs-M1Pi may be induced by an open/closed transition of the active site. The highly conserved residue at the active site, namely Asp240 is most likely to be involved in the reaction mechanism as an acid/base catalyst. The structural analysis sheds light on its catalytic mechanism of M1Pi.

In Chapter II, the purification and preliminary crystallographic studies of *B. subtilis* DK-MTP-1P enolase (Bs-DK-MTP-1P enolase) are reported. The crystal structure of the apo, decarbamylated (E) form of *B. subtilis* DK-MTP-1P enolase (Bs-DK-MTP-1P enolase) has been also determined at 2.3 Å resolution. To date, the crystal structures of four different forms of *Geobacillus kaustophilus* DK-MTP-1P enolase (Gk-DK-MTP-1P enolase; 60% sequence identity)

have been reported: the PO_4^{3-}-bound decarbamylated form (E-PO_4^{3-}), the carbamylated (activated) form complexed with Mg^{2+} (ECM), and the ECM forms complexed with bicarbonate (ECM-HCO_3^-), or alternate substrate 2,3-diketohexane-1-phosphate (ECM-substrate). On the other hand, structures of RuBisCOs have been extensively studied for various forms; including E-, E-ligand-, ECM-, and ECM-ligand-forms. The structural comparison between DK-MTP-1P enolase and RuBisCO in the discrete catalytic steps, revealed that Lys150 (equivalent to Lys175 in RuBisCO) adopts an induced fit to the active site. This unusual conformational change appears to be induced by changes in the φ and Ψ angles of Gly151, which is well conserved in the sequences of Bs- and Gk-DK-MTP-1P enolases but not in those of RuBisCOs. As for the loop at 303-312, equivalent to the catalytic loop termed "loop-6" in RuBisCO, the loop possesses a closed conformation in the E-form of Bs-DK-MTP-1P enolase. The closed conformation is stabilized by Pro312, which is conserved in the sequences of several RLPs (equivalent to Glu338 in RuBisCO). Then, we discuss the common structurally stabilization of loop-6 between Bs-DK-MTP-1P enolase and a high CO_2-fixation RuBisCO.

As the future work, the enzymatic activities of RuBisCO need to be measured in order to examine the effects of site-specific mutations, which lead to stabilize loop-6 in the closed conformation. Additionally, the detailed X-ray structural analyses for these mutated enzymes will be required to explain how the stabilization of loop-6 affects a high CO_2 fixation. Based on these results, a new turn will began to create super RuBisCO with higher $S_{C/O}$, realizing the sustainable development on the earth.

References

1. Rando, R.R. 1996. Chemical biology of isoprenylation/methylation, *Biochem. Soc. Trans.* **24**, 682-687.

2. Williams-Ashman, H.G., and Canellakis, Z.N. 1979. Polyamines in mammalian biology and medicine, *Perspect. Biol. Med.* **22**, 421-453.

3. Trackman, P.C., and Abeles, R.H. 1983. Methionine synthesis from 5'-S-Methylthioadenosine. Resolution of enzyme activities and identification of 1-phospho-5-S methylthioribulose, *J. Biol. Chem.* **258**, 6717-6720.

4. Sekowska, A., Denervaud, V., Ashida, H., Michoud, K., Haas, D., Yokota, A., and Danchin, A. 2004. Bacterial variations on the methionine salvage pathway, *BMC Microbiol.* **4**, 9.

5. Pirkov, I., Norbeck, J., Gustafsson, L., and Albers, E. 2008. A complete inventory of all enzymes in the eukaryotic methionine salvage pathway, *FEBS J.* **275**, 4111-4120.

6. Christopher, S.A., Diegelman, P., Porter, C.W., and Kruger, W.D. 2002. Methylthioadenosine phosphorylase, a gene frequently codeleted with p16(cdkN2a/ARF), acts as a tumor suppressor in a breast cancer cell line, *Cancer Res.* **62**, 6639-6644.

7. Ashida, H., Saito, Y., Kojima, C., Kobayashi, K., Ogasawara, N., and Yokota, A. 2003. A functional link between RuBisCO-like protein of Bacillus and photosynthetic RuBisCO, *Science* **302**, 286-290.

8. Sekowska, A., and Danchin, A. 2002. The methionine salvage pathway in Bacillus subtilis, *BMC Microbiol.* **2**, 8.

9. Lorimer, G.H. 1981. *Annu. Rev. Plant. Biol.* **32**, 349-383.

10. Imker, H.J., Fedorov, A.A., Fedorov, E.V., Almo, S.C., and Gerlt, J.A. 2007. Mechanistic Diversity in the RuBisCO Superfamily: The "Enolase" in the Methionine Salvage Pathway in *Geobacillus kaustophilus*, *Biochemistry (Mosc).* **46**, 4077-4089.

11. Rose, I.A. 1975. Mechanism of the aldose-ketose isomerase reactions, *Adv. Enzymol. Relat. Areas Mol.*

Biol. **43**, 491-517.

12. Topper, Y.J. 1957. On the mechanism of action of phosphoglucose isomerase and phosphomannose isomerase, *J. Biol. Chem.* **225**, 419-425.

13. Rose, I.A., and O'Connell, E.L. 1960. Stereospecificity of the sugarphosphate isomerase reactions; a uniformity, *Biochim. Biophys. Acta* **42**, 159-160.

14. Fenn, T.D., Ringe, D., and Petsko, G.A. 2004. Xylose isomerase in substrate and inhibitor michaelis states: atomic resolution studies of a metal-mediated hydride shift, *Biochemistry* **43**, 6464-6474.

15. Blow, D.M., Collyer, C.A., Goldberg, J.D., and Smart, O.S. 1992. Structure and mechanism of D-xylose isomerase, *Faraday Discuss.*, 67-73.

16. Asboth, B., and Naray-Szabo, G. 2000. Mechanism of action of D-xylose isomerase, *Curr Protein Pept Sci.* **1**, 237-254.

17. Saito, Y., Ashida, H., Kojima, C., Tamura, H., Matsumura, H., Kai, Y., and Yokota, A. 2007. Enzymatic characterization of 5-methylthioribose 1-phosphate isomerase from *Bacillus subtilis*, *Biosci.Biotechno. Biochem*. **71**, 2021-2028.

18. Bateman, A., Coin, L., Durbin, R., Finn, R.D., Hollich, V., Griffiths-Jones, S., Khanna, A., Marshall, M., Moxon, S., Sonnhammer, E.L., et al. 2004. The Pfam protein families database, *Nucleic. Acids Res.* **32**, D138-141.

19. Price, N., and Proud, C. 1994. The guanine nucleotide-exchange factor, eIF-2B, *Biochimie* **76**, 748-760.

20. Kyrpides, N.C., and Woese, C.R. 1998. Archaeal translation initiation revisited: the initiation factor 2 and eukaryotic initiation factor 2B alpha-beta-delta subunit families, *Proc. Natl. Acad. Sci. U. S. A.* **95**, 3726-3730.

21. Berman, H.M., Westbrook, J., Feng, Z., Gilliland, G., Bhat, T.N., Weissig, H., Shindyalov, I.N., and Bourne, P.E. 2000. The Protein Data Bank, *Nucleic. Acids Res.* **28**, 235-242.

22. Bumann, M., Djafarzadeh, S., Oberholzer, A.E., Bigler, P., Altmann, M., Trachsel, H., and Baumann, U.

2004. Crystal structure of yeast Ypr118w, a methylthioribose-1-phosphate isomerase related to regulatory eIF2B subunits, *J. Biol. Chem.* **279**, 37087-37094.

23. Kakuta, Y., Tahara, M., Maetani, S., Yao, M., Tanaka, I., and Kimura, M. 2004. Crystal structure of the regulatory subunit of archaeal initiation factor 2B (aIF2B) from hyperthermophilic archaeon Pyrococcus horikoshii OT3: a proposed structure of the regulatory subcomplex of eukaryotic IF2B, *Biochem. Biophys. Res. Commun.* **319**, 725-732.

24. Saito, Y., Ashida, H., Kojima, C., Tamura, H., Matsumura, H., Kai, Y., and Yokota, A. 2007. Enzymatic characterization of 5-methylthioribose 1-phosphate isomerase from Bacillus subtilis, *Biosci. Biotechnol. Biochem.* **71**, 2021-2028.

25. Otwinowski, Z., Minor, W. 1997. Processing of X-ray Diffraction Data Collected in Oscillation Mode, *Methods Enzymol.* **276**, 307-326.

26. 1994. The CCP4 suite: programs for protein crystallography, *Acta Crystallogr. D. Biol. Crystallogr.* **50**, 760-763.

27. Otwinowski, Z. 1993. Proceedings of the CCP4 Study Weekend: Data Collection and Processing, edited by L. Sawyer, N. Isaacs and S. Bailey, pp. 56-62. Warrington: Daresbury Laboratory.

28. Vagin, A., and Teplyakov, A. 1997. MOLREP: an automated program for molecular replacement., *J. Appl. Cryst.* **30**, 1022-1025.

29. Adams, P.D., Pannu, N.S., Read, R.J., and Brunger, A.T. 1997. Cross-validated maximum likelihood enhances crystallographic simulated annealing refinement, *Proc. Natl. Acad. Sci. U S A* **94**, 5018-5023.

30. Emsley, P., and Cowtan, K. 2004. Coot: model-building tools for molecular graphics, *Acta Crystallogr. D Biol. Crystallogr.* **60**, 2126-2132.

31. Laskowski, R.A., MacArthur, M.W., Moss, D.S., and Thornton, J.M. 1993. PROCHECK: a program to check the stereochemical quality of protein structures, *J. Appl. Cryst.* **26**, 283-291.

32. Hooft, R.W.W., Vriend, G., Sander, C., and Abola, E.E. 1996. Errors in protein structures, *Nature* **381**, 272-272.

33. Kraulis, P.J. 1991. MOLSCRIPT: a program to produce both detailed and schematic plots of protein structures., *J. Appl. Crystallogr.* **24**, 946-950.

34. Merritt, E.A. 1994. Raster3D Version 2.0. A program for photorealistic molecular graphics, *Acta Crystallogr. D Biol. Crystallogr.* **50**, 869-873.

35. DeLano, W.L. 2002. The PyMOL Molecular Graphics System.

36. Nicholls, A., Sharp, K.A., and Honig, B. 1991. Protein folding and association: insights from the interfacial and thermodynamic properties of hydrocarbons, *Proteins* **11**, 281-296.

37. Naor, M.M., and Jensen, J.H. 2004. Determinants of cysteine pKa values in creatine kinase and alpha1-antitrypsin, *Proteins* **57**, 799-803.

38. Mehler, E.L., Fuxreiter, M., Simon, I., and Garcia-Moreno, E.B. 2002. The role of hydrophobic microenvironments in modulating pKa shifts in proteins, *Proteins* **48**, 283-292.

39. Inoue, M., Yamada, H., Hashimoto, Y., Yasukochi, T., Hamaguchi, K., Miki, T., Horiuchi, T., and Imoto, T. 1992. Stabilization of a protein by removal of unfavorable abnormal pKa: substitution of undissociable residue for glutamic acid-35 in chicken lysozyme, *Biochemistry* **31**, 8816-8821.

40. Langsetmo, K., Fuchs, J.A., and Woodward, C. 1991. The conserved, buried aspartic acid in oxidized Escherichia coli thioredoxin has a pKa of 7.5. Its titration produces a related shift in global stability, *Biochemistry* **30**, 7603-7609.

41. Hayward, S., and Berendsen, H.J. 1998. Systematic analysis of domain motions in proteins from conformational change: new results on citrate synthase and T4 lysozyme, *Proteins* **30**, 144-154.

42. Keeble, A.H., Kirkpatrick, N., Shimizu, S., and Kleanthous, C. 2006. Calorimetric dissection of colicin DNase--immunity protein complex specificity, *Biochemistry (Mosc).* **45**, 3243-3254.

43. Farber, G.K., Glasfeld, A., Tiraby, G., Ringe, D., and Petsko, G.A. 1989. Crystallographic studies of the

mechanism of xylose isomerase, *Biochemistry* **28**, 7289-7297.

44. Collyer, C.A., Henrick, K., and Blow, D.M. 1990. Mechanism for aldose-ketose interconversion by D-xylose isomerase involving ring opening followed by a 1,2-hydride shift, *J. Mol. Biol.* **212**, 211-235.

45. Andrews, T.J., and Lorimer, G.H. 1987. *in: M.D. Hatch, N.K. Bordman (Eds.), The biochemistry of plants, academic press, New York*, 131-218.

46. Hartman, F.C., and Harpel, M.R. 1994. Structure, function, regulation, and assembly of D-ribulose-1,5-bisphosphate carboxylase/oxygenase, *Annu. Rev. Biochem.* **63**, 197-234.

47. Cleland, W.W., Andrews, T.J., Gutteridge, S., Hartman, F.C., and Lorimer, G.H. 1998. Mechanism of Rubisco: The Carbamate as General Base, *Chem. Rev.* **98**, 549-562.

48. Von Caemmerer, S., Millgate, A., Farquhar, G.D., and Furbank, R.T. 1997. Reduction of Ribulose-1,5-Bisphosphate Carboxylase/Oxygenase by Antisense RNA in the C4 Plant Flaveria bidentis Leads to Reduced Assimilation Rates and Increased Carbon Isotope Discrimination, *Plant Physiol.* **113**, 469-477.

49. Hudson, G.S., Evans, J.R., von Caemmerer, S., Arvidsson, Y.B., and Andrews, T.J. 1992. Reduction of Ribulose-1,5-Bisphosphate Carboxylase/Oxygenase Content by Antisense RNA Reduces Photosynthesis in Transgenic Tobacco Plants, *Plant Physiol.* **98**, 294-302.

50. Ellis, R.J. 1979. The most abundant protein in the world, *Trends Biochem. Sci.* **4**, 241-244.

51. Curmi, P.M., Cascio, D., Sweet, R.M., Eisenberg, D., and Schreuder, H. 1992. Crystal structure of the unactivated form of ribulose-1,5-bisphosphate carboxylase/oxygenase from tobacco refined at 2.0-A resolution, *J. Biol. Chem.* **267**, 16980-16989.

52. Schneider, G., Lindqvist, Y., and Lundqvist, T. 1990. Crystallographic refinement and structure of ribulose-1,5-bisphosphate carboxylase from Rhodospirillum rubrum at 1.7 A resolution, *J. Mol. Biol.* **211**, 989-1008.

53. Lundqvist, T., and Schneider, G. 1991. Crystal structure of the ternary complex of ribulose-1,5-bisphosphate carboxylase, Mg(II), and activator CO_2 at 2.3-A resolution, *Biochemistry (Mosc).* **30**, 904-908.

54. Taylor, T.C., and Andersson, I. 1997. Structure of a product complex of spinach ribulose-1,5-bisphosphate carboxylase/oxygenase, *Biochemistry (Mosc).* **36**, 4041-4046.

55. Duff, A.P., Andrews, T.J., and Curmi, P.M. 2000. The transition between the open and closed states of rubisco is triggered by the inter-phosphate distance of the bound bisphosphate, *J. Mol. Biol.* **298**, 903-916.

56. Suh, S.W., Cascio, D., Chapman, M.S., and Eisenberg, D. 1987. A crystal form of ribulose-1,5-bisphosphate carboxylase/oxygenase from Nicotiana tabacum in the activated state, *J. Mol. Biol.* **197**, 363-365.

57. Hansen, S., Vollan, V.B., Hough, E., and Andersen, K. 1999. The crystal structure of rubisco from Alcaligenes eutrophus reveals a novel central eight-stranded beta-barrel formed by beta-strands from four subunits, *J. Mol. Biol.* **288**, 609-621.

58. Okano, Y., Mizohata, E., Xie, Y., Matsumura, H., Sugawara, H., Inoue, T., Yokota, A., and Kai, Y. 2002. X-ray structure of Galdieria Rubisco complexed with one sulfate ion per active site, *FEBS Lett.* **527**, 33-36.

59. Newman, J., and Gutteridge, S. 1993. The X-ray structure of Synechococcus ribulose-bisphosphate carboxylase/oxygenase-activated quaternary complex at 2.2-A resolution, *J. Biol. Chem.* **268**, 25876-25886.

60. Zhang, K.Y., Cascio, D., and Eisenberg, D. 1994. Crystal structure of the unactivated ribulose 1,5-bisphosphate carboxylase/oxygenase complexed with a transition state analog, 2-carboxy-D-arabinitol 1,5-bisphosphate, *Protein Sci.* **3**, 64-69.

61. Taylor, T.C., Fothergill, M.D., and Andersson, I. 1996. A common structural basis for the inhibition of

ribulose 1,5-bisphosphate carboxylase by 4-carboxyarabinitol 1,5-bisphosphate and xylulose 1,5-bisphosphate, *J. Biol. Chem.* **271**, 32894-32899.

62. Taylor, T.C., and Andersson, I. 1997. The structure of the complex between rubisco and its natural substrate ribulose 1,5-bisphosphate, *J. Mol. Biol.* **265**, 432-444.

63. Sugawara, H., Yamamoto, H., Shibata, N., Inoue, T., Okada, S., Miyake, C., Yokota, A., and Kai, Y. 1999. Crystal structure of carboxylase reaction-oriented ribulose 1, 5-bisphosphate carboxylase/oxygenase from a thermophilic red alga, *Galdieria partita*, *J. Biol. Chem.* **274**, 15655-15661.

64. Newman, J., and Gutteridge, S. 1994. Structure of an effector-induced inactivated state of ribulose 1,5-bisphosphate carboxylase/oxygenase: the binary complex between enzyme and xylulose 1,5-bisphosphate, *Structure* **2**, 495-502.

65. Shibata, N., Inoue, T., Fukuhara, K., Nagara, Y., Kitagawa, R., Harada, S., Kasai, N., Uemura, K., Kato, K., Yokota, A., et al. 1996. Orderly disposition of heterogeneous small subunits in D-ribulose-1,5-bisphosphate carboxylase/oxygenase from spinach, *J. Biol. Chem.* **271**, 26449-26452.

66. Andersson, I. 1996. Large structures at high resolution: the 1.6 A crystal structure of spinach ribulose-1,5-bisphosphate carboxylase/oxygenase complexed with 2-carboxyarabinitol bisphosphate, *J. Mol. Biol.* **259**, 160-174.

67. Taylor, T.C., Backlund, A., Bjorhall, K., Spreitzer, R.J., and Andersson, I. 2001. First crystal structure of Rubisco from a green alga, *Chlamydomonas reinhardtii*, *J. Biol. Chem.* **276**, 48159-48164.

68. Mizohata, E., Matsumura, H., Okano, Y., Kumei, M., Takuma, H., Onodera, J., Kato, K., Shibata, N., Inoue, T., Yokota, A., et al. 2002. Crystal structure of activated ribulose-1,5-bisphosphate carboxylase/oxygenase from green alga *Chlamydomonas reinhardtii* complexed with 2-carboxyarabinitol-1,5-bisphosphate, *J. Mol. Biol.* **316**, 679-691.

69. Lundqvist, T., and Schneider, G. 1991. Crystal structure of activated ribulose-1,5-bisphosphate carboxylase complexed with its substrate, ribulose-1,5-bisphosphate, *J. Biol. Chem.* **266**,

12604-12611.

70. Saunders, N.F., Thomas, T., Curmi, P.M., Mattick, J.S., Kuczek, E., Slade, R., Davis, J., Franzmann, P.D., Boone, D., Rusterholtz, K., et al. 2003. Mechanisms of thermal adaptation revealed from the genomes of the Antarctic Archaea *Methanogenium frigidum* and *Methanococcoides burtonii*, *Genome Res.* **13**, 1580-1588.

71. Schneider, G., Lindqvist, Y., and Branden, C.I. 1992. RUBISCO: structure and mechanism, *Annu. Rev. Biophys. Biomol. Struct.* **21**, 119-143.

72. Schreuder, H.A., Knight, S., Curmi, P.M., Andersson, I., Cascio, D., Branden, C.I., and Eisenberg, D. 1993. Formation of the active site of ribulose-1,5-bisphosphate carboxylase/oxygenase by a disorder-order transition from the unactivated to the activated form, *Proc. Natl. Acad. Sci. U. S. A.* **90**, 9968-9972.

73. Kunst, F., Ogasawara, N., Moszer, I., Albertini, A.M., Alloni, G., Azevedo, V., Bertero, M.G., Bessieres, P., Bolotin, A., Borchert, S., et al. 1997. The complete genome sequence of the gram-positive bacterium *Bacillus subtilis*, *Nature* **390**, 249-256.

74. Hanson, T.E., and Tabita, F.R. 2001. A ribulose-1,5-bisphosphate carboxylase/oxygenase (RubisCO)-like protein from *Chlorobium tepidum* that is involved with sulfur metabolism and the response to oxidative stress, *Proc. Natl. Acad. Sci.* **98**, 4397-4402.

75. Ashida, H., Danchin, A., and Yokota, A. 2005. Was photosynthetic RuBisCO recruited by acquisitive evolution from RuBisCO-like proteins involved in sulfur metabolism?, *Res. Microbiol.* **156**, 611-618.

76. Ashida, H., Saito, Y., Nakano, T., Tandeau de Marsac, N., Sekowska, A., Danchin, A., and Yokota, A. 2008. RuBisCO-like proteins as the enolase enzyme in the methionine salvage pathway: functional and evolutionary relationships between RuBisCO-like proteins and photosynthetic RuBisCO, *J. Exp. Bot.* **59**, 1543-1554.

77. Tabita, F.R., Satagopan, S., Hanson, T.E., Kreel, N.E., and Scott, S.S. 2008. Distinct form I, II, III, and IV Rubisco proteins from the three kingdoms of life provide clues about Rubisco evolution and structure/function relationships, *J. Exp. Bot.* **59**, 1515-1524.

78. Carre-Mlouka, A., Mejean, A., Quillardet, P., Ashida, H., Saito, Y., Yokota, A., Callebaut, I., Sekowska, A., Dittmann, E., Bouchier, C., et al. 2006. A new rubisco-like protein coexists with a photosynthetic rubisco in the planktonic cyanobacteria Microcystis, *J. Biol. Chem.* **281**, 24462-24471.

79. Winans, S.C., and Bassler, B.L. 2002. Mob psychology, *J. Bacteriol.* **184**, 873-883.

80. Imker, H.J., Singh, J., Warlick, B.P., Tabita, F.R., and Gerlt, J.A. 2008. Mechanistic diversity in the RuBisCO superfamily: a novel isomerization reaction catalyzed by the RuBisCO-like protein from *Rhodospirillum rubrum*, *Biochemistry (Mosc).* **47**, 11171-11173.

81. Li, H., Sawaya, M.R., Tabita, F.R., and Eisenberg, D. 2005. Crystal structure of a RuBisCO-like protein from the green sulfur bacterium *Chlorobium tepidum*, *Structure* **13**, 779-789.

82. Tabita, F.R., Hanson, T.E., Li, H., Satagopan, S., Singh, J., and Chan, S. 2007. Function, structure, and evolution of the RubisCO-like proteins and their RubisCO homologs, *Microbiol. Mol. Biol. Rev.* **71**, 576-599.

83. Lorimer, G.H. 1981. Ribulosebisphosphate carboxylase: amino acid sequence of a peptide bearing the activator carbon dioxide, *Biochemistry (Mosc).* **20**, 1236-1240.

84. Lorimer, G.H., and Miziorko, H.M. 1980. Carbamate formation on the epsilon-amino group of a lysyl residue as the basis for the activation of ribulosebisphosphate carboxylase by CO_2 and Mg^{2+}, *Biochemistry (Mosc).* **19**, 5321-5328.

85. Lorimer, G.H., Chen, Y.R., and Hartman, F.C. 1993. A role for the epsilon-amino group of lysine-334 of ribulose-1,5-bisphosphate carboxylase in the addition of carbon dioxide to the 2,3-enediol(ate) of ribulose 1,5-bisphosphate, *Biochemistry (Mosc).* **32**, 9018-9024.

86. Miziorko, H.M., and Sealy, R.C. 1980. Characterization of the ribulosebisphosphate carboxylase-carbon

dioxide-divalent cation-carboxypentitol bisphosphate complex, *Biochemistry (Mosc).* **19**, 1167-1171.

87. Pierce, J., and Reddy, G.S. 1986. The sites for catalysis and activation of ribulosebisphosphate carboxylase share a common domain, *Arch. Biochem. Biophys.* **245**, 483-493.

88. Gill, S.C., and von Hippel, P.H. 1989. Calculation of protein extinction coefficients from amino acid sequence data, *Anal. Biochem.* **182**, 319-326.

89. Matthews, B.W. 1968. Solvent content of protein crystals, *J. Mol. Biol.* **33**, 491-497.

90. Collaborative Computational Project, N. 1994. The CCP4 suite: programs for protein crystallography, *Acta Crystallogr. D. Biol. Crystallogr.* **50**, 760-763.

91. Leslie, A.G. 2006. The integration of macromolecular diffraction data, *Acta Crystallogr. D. Biol. Crystallogr.* **62**, 48-57.

92. Vagin, A., Teplyakov, A. 1997. MOLREP: an automated program for molecular replacement, *J.Appl.Cryst.* **30**, 1022-1025.

93. Uemura, K., Anwaruzzaman, Miyachi, S., and Yokota, A. 1997. Ribulose-1,5-bisphosphate carboxylase/oxygenase from thermophilic red algae with a strong specificity for CO_2 fixation, *Biochem. Biophys. Res. Commun.* **233**, 568-571.

List of Publication

1. Crystallization and preliminary X-ray analysis of methylthioribose-1-phosphate isomerase from *Bacillus subtilis*.

Haruka Tamura, Hiroyoshi Matsumura, Tsuyoshi Inoue, Hiroki Ashida, Yohtaro Saito, Akiho Yokota, and Yasushi Kai.

Acta Crystallographica Section F, (2005), Vol.61, No.6, pp595-598.

2. Crystal structure of 5-methylthioribose 1-phosphate isomerase product complex from *Bacillus subtilis*: implications for catalytic mechanism.

Haruka Tamura, Yohtaro Saito, Hiroki Ashida, Tsuyoshi Inoue, Yasushi Kai, Akiho Yokota, and Hiroyoshi Matsumura.

Protein Science, (2008), Vol.17, pp126-135.

3. Crystallization and preliminary X-ray analysis of 2,3-diketo-5-methylthiopentyl-1-phosphate enolase from *Bacillus subtilis*.

Haruka Tamura, Hiroki Ashida, Shogo Koga, Yohtaro Saito, Tomonori Yadani, Yasushi Kai, Tsuyoshi Inoue, Akiho Yokota, and Hiroyoshi Matsumura.

Acta Crystallographica Section F, Vol.65, No.2, pp147-150.

4. Crystal structure of the apo, decarbamylated form of 2,3-diketo-5-methylthiopentyl-1- phosphate enolase from *Bacillus subtilis*.

Haruka Tamura, Yohtaro Saito, Hiroki Ashida, Yasushi Kai, Tsuyoshi Inoue, Akiho Yokota, and Hiroyoshi Matsumura.

Acta Crystallographica Section D, submitted.

Supplementary publication

1. Enzymatic characterization of 5-methylthioribose 1-phosphate isomerase from *Bacillus subtilis*.

Yohtaro Saito, Hiroki Ashida, Chojiro Kojima, Haruka Tamura, Hiroyoshi Matsumura, Yasushi Kai, and Akiho Yokota.

Bioscience, Biotechnology, and Biochemistry, (2007), Vol71, pp2021-2028.

Acknowledgement

The author wishes to express her special gratitude to Prof. Yasushi Kai, Prof. Susumu Kuwabata, and Prof. Tsuyoshi Inoue for their enthusiastic guidance, helpful suggestion, and encouragement throughout the studies. The author sincerely appreciates Associate Prof. Hiroyoshi Matsumura for his stimulating discussion and interesting suggestion for the accomplishment of this work. She acknowledges Lecturer Nobuko Kanehisa for her kind encouragement and helpful advice.

In Chapter I, the author is grateful to Dr. K. Hasegawa and Dr. H. Sakai at BL38B1 (SPring-8), and to Dr. A. Nakagawa and Dr. E. Yamashita, Institute for Protein Research, Osaka University, at BL44XU (SPring-8) for their kind help in the data collection. The synchrotron radiation experiments were performed at SPring-8 with the approval of the Japan Synchrotron Radiation Research Institute (JASRI) (2005A0805-NL1-np-P3k), and Institute for Protein Research, Osaka University (C04A44XU-7119-N).

In Chapter II, the synchrotron radiation experiments were performed at SPring-8 with Institute for Protein Research, Osaka University (2006B6806). The author is grateful to Prof. A. Nakagawa, Dr. E. Yamashita, and Dr. M. Yoshimura, Institute for Protein Research, Osaka University, at BL44XU (SPring-8) for their kind help in the data collection.

Special thanks are given to the author's co-workers Mr. Shogo Koga, Mrs. Ikue Sakaguchi, Mr. Tomonori Yadani, Mr. Takeshi Ueno for their stimulating and fruitful cooperation. The author expresses her special thanks to the Research Fellowships of the Japan Society for the Promotion of Science for Young Scientists, Science and Technology Incubation Program; and the Global COE program from the Japanese Ministry of Education, Culture, Sports, Science and Technology. The author apologizes to colleagues whose work she is not able to describe because of space limitation.